Keldysh Institute • Publication search

Keldysh Institute preprints • Preprint No. 8, 2010

T. Beuselinck, C. Van Bavinchove,
Sazonov V.V.

Quasi-steady Accelerations Onboard FOTON M-3 Spacecraft

Recommended form of bibliographic references: T. Beuselinck, C. Van Bavinchove, Sazonov V.V. Quasi-steady Accelerations Onboard FOTON M-3 Spacecraft. Keldysh Institute preprints, 2010, No. 8, 36 p. URL: **http://library.keldysh.ru/preprint.asp?id=2010-8&lg=e**

RUSSIAN ACADEMY OF SCIENCES
KELDYSH INSTITUTE OF APPLIED MATHEMATICS

T. Beuselinck, C. Van Bavinchove, V.V. Sazonov

QUASI-STEADY ACCELERATIONS ONBOARD FOTON M-3 SPACECRAFT

Moscow - 2010

Annotation

The paper presents the results of the full reconstruction of the attitude motion of the spacecraft *Foton M-3* during its uncontrolled flight in September 14 — 24, 2007. The motion was reconstructed in the form of solutions of appropriate spacecraft motion equations. We found the solutions by processing onboard measurements of the Earth magnetic field strength. The measurement data were accumulated continually during the whole flight but the processing procedure dealt with data segments, which had length about a few hours. The measurement data on each such segment were processed simultaneously by means of the least squares method and integration of the spacecraft motion equations. This approach gives us the solution that provided the best approximation of measurement data. We adopted the solution as a motion reconstruction in the considered time segment. Then we certain calculated functions along this solution, which allow to calculate quasi-steady accelerations at any point of the spacecraft body. We check our description by comparing the functions found in overlapping data segments.

Т. Бойзелинк, К. Ван Бавинхов, В.В. Сазонов. Квазистатические микроускорения на борту космического аппарата "Фотон М-3". Приведены результаты полной реконструкции вращательного движения КА "Фотон М-3" в его неуправляемом полете 14 — 24 сентября 2007 г. Реконструкция выполнена в виде решений уравнений движения КА, причем решения находились в результате обработки выполненных на борту измерений магнитного поля Земли. Измерения выполнялись в течение всего полета, но их обработка выполнялась порциями, охватывающими отрезки времени длиной в несколько часов. На каждом таком отрезке данные измерений обрабатывались совместно методом наименьших квадратов с помощью интегрирования уравнений движения КА относительно центра масс. При обработке оценивались начальные условия движения и параметры используемой математической модели. Решения, построенные таким образом на перекрывающихся отрезках времени, позволили восстановить реальное вращательное движение КА в течение всего неуправляемого полета. Рассогласования решений на пересечениях смежных отрезков дали оценки точности построенной реконструкции. На основании этой реконструкции проведены расчеты квазистатических микроускорений на борту КА.

1. Description of quasi-steady accelerations in *Foton M-3*. We start from the following definition. Let a spacecraft be a rigid body and let a point P be fixed with its frame. The difference between the gravitational field strength at the point P and the absolute acceleration of this point is called a residual acceleration at the point P. We denote the difference by $\mathbf{b}$. If a small mass m is fixed at the point P, then the mass undergoes the reaction force $-m\mathbf{b}$ from the spacecraft. We assume that only the atmosphere drag is significant among nongravitational actions upon the spacecraft. Then $\mathbf{b}$ is defined by the well-known formula [1]

$$\mathbf{b} = \mathbf{r} \times \dot{\boldsymbol{\omega}} + (\boldsymbol{\omega} \times \mathbf{r}) \times \boldsymbol{\omega} + \chi \left[3 \left(\mathbf{e} \cdot \mathbf{r}\right) \mathbf{e} - \mathbf{r}\right] + \mathbf{b}_a \,, \tag{1}$$

$$\chi = \frac{\mu_e}{|\mathbf{R}|^3} \,, \quad \mathbf{e} = \frac{\mathbf{R}}{|\mathbf{R}|} \,, \quad \mathbf{b}_a = c\rho_a |\mathbf{v}| \mathbf{v} \,.$$

Here, $\mathbf{r} = \overrightarrow{OP}$; the point O is the spacecraft center of mass; $\boldsymbol{\omega}$ is the absolute angular rate of the spacecraft; the dot above a symbol denotes differentiation with respect to time t; μ_e is the gravitational parameter of the Earth; $\mathbf{R}$ is the geocentric radius vector of the point O; $\mathbf{v}$ is the velocity of the point O with respect to the Earth surface; ρ_a is the atmosphere density at the point O; c is the spacecraft ballistic coefficient.

If we reconstructed a real spacecraft motion basing on a certain information and found the functions $\boldsymbol{\omega}(t)$, $\dot{\boldsymbol{\omega}}(t)$, $\chi(t)$, $\mathbf{e}(t)$, and $\mathbf{b}_a(t)$, then we can calculate the real acceleration $\mathbf{b}(t)$ at any point P by formula (1). This formula was derived for a general situation without any frequency restrictions. But if the spacecraft was large like *Fotons* and if we reconstructed its real attitude motion as a motion of a rigid body (this motion is usually very slow), then formula (1) gives only a quasi-steady acceleration component, i.e., a part of a real acceleration that has frequencies within the range from 0 to 0.01 Hz. A special investigation of quasi-steady accelerations is expedient because they alone are the most important in many space experiments.

We have to use a coordinate system to specify the vectors $\boldsymbol{\omega}$, $\dot{\boldsymbol{\omega}}$, $\mathbf{e}$, and $\mathbf{b}_a$ in explicit form. We use below the structural ($\equiv$ device) coordinate system $Ox_1x_2x_3$ of *Foton M-3*. The point O is its origin; the axes Ox_1, Ox_2, and Ox_3 are directed parallel to the axes $(-x)$, y and $(-z)$ of the usual capsula coordinate system. We suppose the vectors above have the following form in the system $Ox_1x_2x_3$: $\boldsymbol{\omega} = (\omega_1, \omega_2, \omega_3)$, $\dot{\boldsymbol{\omega}} = (\dot{\omega}_1, \dot{\omega}_2, \dot{\omega}_3)$, $\mathbf{e} = (e_1, e_2, e_3)$, $\mathbf{b}_a = (b_{a1}, b_{a2}, b_{a3})$.

The attitude motion of *Foton M-3* was reconstructed in terms of solutions of the spacecraft motion equations [2]. We found such solutions by processing onboard measurements of the Earth magnetic field strength. The measurement data were accumulated continually during the whole flight (within the period September 14 — 25, 2007), but the processing procedure dealt with data segments, which had length about a few hours. The measurement data in each such

segment were processed simultaneously by means of the least squares method and integration of the spacecraft motion equations [2]. The purpose of processing was to find a solution that provided the best approximation of the measurement data. The estimates of the equation parameters and initial conditions of the solution were obtained as a result of such processing. Those quantities allowed us to calculate the solution of the motion equations that was declared to be a motion reconstruction in the considered time segment.

After the required solution was found, we calculated along it the quantities ω_i, $\dot{\omega}_i$, e_i, b_{ai} $(i = 1, 2, 3)$, and χ in points of a certain time grid and wrote the results in a file corresponding to the processed data segment. In that way, we obtained a set of files, which covered (with overlaps) the uncontrolled flight of *Foton M-3*. This set of files gives the full description of quasi-steady accelerations onboard the spacecraft. We describe below some aspects of the used calculation procedures and demonstrate the data obtained.

2. Mathematical model of spacecraft attitude motion. The spacecraft is assumed to be a gyrostat. To write equations of its motion and relations, used in processing measurement data, we introduce two right-hand Cartesian coordinate systems.

The system $Ox_1x_2x_3$ was already mentioned above. It is used for interpretation of measurement data implemented by various onboard sensors. We assume here additionally that its axes are the spacecraft principal central axes of inertia. All vector components and coordinates of points refer below to the system $Ox_1x_2x_3$ unless specifically stated to the contrary.

The Greenwich system $CY_1Y_2Y_3$ is connected with the Earth. Its origin is in the Earth center; the plane CY_1Y_2 coincides with the equator plane; the axis CY_1 intersects the Greenwich meridian, the axis CY_3 is directed to the North Pole.

We denote the transition matrix from the system $Ox_1x_2x_3$ to the Greenwich system by $\| g_{ij} \|_{i,j=1}^{3}$. Here $g_{ij} = \cos(CY_i \hat{} Ox_j)$. The matrix elements are expressed through the angles γ_g, δ_g, and β_g, which are defined in the following way [2]. The system $CY_1Y_2Y_3$ can be transformed to the system $Ox_1x_2x_3$ by three sequential rotations (we suppose the points O and C coincide): 1) by the angle $\delta_g + \pi/2$ around the axis CY_2, 2) by the angle β_g around the new axis CY_3, 3) by the angle γ_g around the new axis CY_1, which coincides with the axis Ox_1.

The complete system of the spacecraft motion equations consists of two subsystems [2]. The first subsystem describes the motion of the point O; the second one describes the rotation of the system $Ox_1x_2x_3$. The first subsystem is written in Greenwich coordinates taking into account the real Earth gravitational field and the atmosphere drag. The field are represented by the series in terms of solid spherical harmonics up to the order (16,16) inclusive. The atmosphere density are calculated according to the model [3]. The solutions of the first subsystem were found from the condition of the best approximation of NORAD two line elements

for *Foton M-3*.

The second subsystem consists of Poisson's kinematic equations for the first and second rows of the matrix $\| g_{ij} \|$, as well as Euler's dynamic equations for the angular rates ω_i $(i = 1, 2, 3)$. We write Euler's equations taking into account the gravitational and restoring aerodynamic torques, as well as the torque from the Earth magnetic field. Besides, we take into account the internal angular momentum of the spacecraft, i.e., the angular momentum produced by onboard revolving equipment: fans, centrifuge rotors, etc. The gravitational and magnetic torques are described by simple analytical formulas. Calculating the aerodynamic torque, we assume the external envelope of the spacecraft is a sphere, its center being displaced from the spacecraft center of mass. Then we obtain for this torque a simple formula too. The subsystem of the attitude motion has the form

$$
\begin{gathered}
\dot\omega_1 = \mu(\omega_2\omega_3 - \nu x_2 x_3) + k_1\,, \\
\dot\omega_2 = \frac{1-\lambda}{1+\lambda\mu}(\omega_1\omega_3 - \nu x_1 x_3) + \frac{\lambda k_2}{1+\lambda\mu}\,, \\
\dot\omega_3 = -(1-\lambda+\lambda\mu)(\omega_1\omega_2 - \nu x_1 x_2) + \lambda k_3\,, \\
\dot g_{11} = g_{12}\omega_3 - g_{13}\omega_2 + \omega_e g_{21}\,, \quad \dot g_{21} = g_{22}\omega_3 - g_{23}\omega_2 - \omega_e g_{11}\,, \\
\dot g_{12} = g_{13}\omega_1 - g_{11}\omega_3 + \omega_e g_{22}\,, \quad \dot g_{22} = g_{23}\omega_1 - g_{21}\omega_3 - \omega_e g_{12}\,, \\
\dot g_{13} = g_{11}\omega_2 - g_{12}\omega_1 + \omega_e g_{23}\,, \quad \dot g_{23} = g_{21}\omega_2 - g_{22}\omega_1 - \omega_e g_{13}\,, \\
\lambda = \frac{I_1}{I_3}\,, \quad \mu = \frac{I_2 - I_3}{I_1}\,, \quad \nu = \frac{3\mu_e}{R^5}\,, \\
k_1 = \kappa(v_2 p_3 - v_3 p_2) + q_2\omega_3 - q_3\omega_2 + m_2 h_3^\circ - m_3 h_2^\circ\,, \\
k_2 = \kappa(v_3 p_1 - v_1 p_3) + q_3\omega_1 - q_1\omega_3 + m_3 h_1^\circ - m_1 h_3^\circ\,, \\
k_3 = \kappa(v_1 p_2 - v_2 p_1) + q_1\omega_2 - q_2\omega_1 + m_1 h_2^\circ - m_2 h_1^\circ\,, \\
R = \sqrt{x_1^2 + x_2^2 + x_3^2}\,, \quad \kappa = E\rho_a\sqrt{v_1^2 + v_2^2 + v_3^2}\,.
\end{gathered}
\tag{2}
$$

Here, x_i and v_i are the components of the vectors $\mathbf{R}$ and $\mathbf{v}$ (see Section 1); the parameters p_i specify the aerodynamic torque; I_i are the moments of inertia of the spacecraft relative to the axes Ox_i; $q_i I_1$ and $m_i I_1$ are the components of the internal angular momentum of the spacecraft and the spacecraft magnetic dipole moment; ω_e is the angular rate of the Earth rotation; h_i° are the component of $\mathbf{H}$, Earth's magnetic field strength at the point O; ρ_a is the atmosphere density at the same point; E is the scale factor.

The components of $\mathbf{H}$ are calculated by the formulas

$$
h_i^\circ = \sum_{j=1}^{3} H_j g_{ji} \quad (i = 1, 2, 3)\,, \tag{3}
$$

where H_k are the components of $\mathbf{H}$ in the Greenwich coordinate system. The latter quantities are specified by the model IGRF2005. The atmosphere density is calculated according to the model [3]. The parameters of equations (2) and of the atmosphere model are assumed to be constant in an interval of data processing.

We use 1000 s as a unit of time and 1000 km as a unit of length when integrate equations (2) numerically. At that the units of the other quantities are following: $[v_i] = \text{km/s}$, $[\omega_i] = [q_i] = 10^{-3}s^{-1}$, $[p_i] = \text{cm/kg}$, $[m_i] = 10^{-5}\text{g}^{-1/2}\text{cm}^{1/2}\text{s}^{-1}$, $[h_i^\circ] = 0.1\text{g}^{1/2}\text{cm}^{-1/2}\text{s}^{-1} = 0.1\text{Oe}$, $[\varrho_a] = \text{kg/m}^3$, $E = 10^{10}$. The units of m_i and h_i° are given in the CGSM system.

The third row of the transition matrix $\| g_{ij} \|$ is calculated in the integration of (2) as a cross-product of its first and second rows. The variables g_{1i} and g_{2i} are dependent owing to orthogonality of the matrix $\| g_{ij} \|$. Therefore the initial values of g_{1i} and g_{2i} are expressed in terms of the angles γ_g, δ_g, and β_g.

The parameters λ and μ in (2) are considered as known. Their values for *Foton M-3* were estimated in [2]: $\lambda = 0.255$, $\mu = 0.1$. The parameters p_i, q_i, and m_i are estimated by processing measurement data along with initial values of a spacecraft attitude motion, i. e., they are fitted parameters. Equations (2) and some other mathematical models in this paper are simpler than analogous models used in [2]. The main and well-founded simplification consists in the admission of the axes Ox_i as the spacecraft principal central axes of inertia. We did that to reduce the total number of fitted parameters and to avoid the use of a priori information and regularization techniques in statistical procedures.

3. Statistical technique of reconstruction of *Foton M-3* attitude motion by magnetic field measurements. There was the equipment DIMAC onboard *Foton M-3*. It measured the magnetic field inside the capsule during the flight. That field was close to Earth's one and so we used DIMAC measurements for reconstructing the attitude motion of the spacecraft by usual statistical techniques. We described briefly the technique used below (see details in [2]).

Magnetic field measurements, obtained in a time interval $t_0 \le t \le t_0 + T$ of several hours, were processed jointly. First we constructed the discrete Fourier series $\hat{h}_i(t)$ $(i = 1, 2, 3)$ approximating components of the measured magnetic field in the system $Ox_1x_2x_3$ in that interval. The root-mean-square error of each function $\hat{h}_i(t)$ was less usually than 80γ ($1\gamma = 10^{-5}$ Oe). Then we calculated the numbers $t_n = t_0 + nT/N$, $h_i^{(n)} = \hat{h}_i(t_n)$, where $n = 0, 1, \ldots, N$. They served input information for searching a solution of equations (3) describing the real spacecraft motion in the interval $t_0 \le t \le t_0 + T$. We named the values $h_i^{(n)}$ by pseudo-measurements. There were usually $T = 150 \div 360$ min, $T/N \approx 1$ min for *Foton M-3*. In some rare cases we joined a few such sets of pseudo-measurements to cover the interval $t_0 \le t \le t_0 + T$ of interest.

Following the least squares method, we considered a solution of system (2) as reconstruction of the real spacecraft motion in the interval $t_0 \le t \le t_0 + T$ if it

provided minimum to the functional [2]

$$\Phi = \sum_{i=1}^{3} \left\{ \sum_{n=0}^{N} \left[h_i^{(n)} - h_i^{\circ}(t_n) \right]^2 - (N+1)\Delta_i^2 \right\}, \tag{4}$$

$$\Delta_i = \frac{1}{N+1} \sum_{n=0}^{N} \left[h_i^{(n)} - h_i^{\circ}(t_n) \right].$$

Here, the functions $h_i^{\circ}(t)$ are defined by formulas (3), Δ_i are the estimates of constant biases in the pseudo-measurements $h_i^{(n)}$. Functional (4) was minimized over 15 quantities: p_i, m_i, q_i, $\omega_i(t_0)$, $\gamma_g(t_0)$, $\delta_g(t_0)$, and $\beta_g(t_0)$. The first 9 quantities specify system (2); the other quantities specify its solution. We solved the minimization problem by Gauss–Newton's method.

We used appropriate standard deviations to characterize the accuracy of approximating the pseudo-measurements and scattering the fitted quantities. The standard deviations were calculated under the following assumptions: errors in the pseudo-measurements $h_i^{(n)}$ were uncorrelated random variables with the same dispersion, errors in the pseudo-measurements with the same subscript i had the same mean value. Let $\Phi_{\min}$ be the value of functional (4) at its minimum point, C be the matrix of Gauss–Newton's normal equations at that point ($2C$ is approximately equal to the matrix of the quadratic form $d^2\Phi$ at the minimum point of Φ). Then the standard deviation of errors in pseudo-measurements is estimated by the quantity

$$\sigma_H = \sqrt{\frac{\Phi_{\min}}{3N-15}}.$$

The standard deviations of the fitted parameters are equal to the square roots of corresponding diagonal elements of the matrix $\sigma_H^2 C^{-1}$. We quote below estimates of the parameter q_1 only. Their standard deviations are denoted by σ_{q1}.

4. Representation of real attitude motion of *Foton M-3* and quasi-steady accelerations in its board. The technique above was applied for reconstructing the spacecraft motion in 57 time intervals. Some their characteristics are presented in Table 1. The table contains the initial point t_0 of each interval, the number N of points with pseudo-measurements, the name of the file containing the results of processing, the estimates of the parameter q_1 and the standard deviations σ_H, σ_{q1}. Each time interval contains all points of the grid $\{t_n\}_{n=0}^{N}$ and has the length T equal to N minutes. There are only two exclusions. Interval 32 has the length of 360 min and interval 56 has the length of 612 min (see figures bellow). Some measurements were lost in those intervals. Each two neighbor intervals have a common part with the length not less than 10 min. The pairs of intervals (54, 55), (55, 56), and (56, 57) have common parts of a few hours.

The results of processing each data segment were written in a separate text file. The contents of the file are arranged in the following way. The first line contains six numbers: $Year$, $Month$, Day, $Hour$, $Minute$ and $Second$, which specify the initial time point t_0 of the time period presented in the file. The numbers $Year$, $Month$, Day, $Hour$ and $Minute$ are integers, the number $Second$ is real. We used the scale UTC for specifying the time. The numbers $Year$ and $Month$ are equal 2007 and 9 in all files, Day is equal 14, 15, 16, ..., 24. Each subsequent line of the file contains values of the quantities: $t-t_0$, ω_1, ω_2, ω_3, $\dot\omega_1$, $\dot\omega_2$, $\dot\omega_3$, e_1, e_2, e_3, χ, b_{a1}, b_{a2}, b_{a3}, h_1°, h_2°, h_3° (quantities (3) need for processing DIMAC measurement data). The quantities ω_i, $\dot\omega_i$, e_i, χ and h_i° in the line are referred to the instant t. The units of these quantities are following: $[t] = 10^3\,\mathrm{s}$, $[\omega_i] = 10^{-3}\,\mathrm{s}^{-1}$, $[\dot\omega_i] = [\chi] = 10^{-6}\,\mathrm{s}^{-2}$, $[b_{ai}] = 10^{-6}\,\mathrm{m/s}^{-2}$, $[h_i^\circ] = \gamma$. The time $t - t_0$ in lines changes with the constant step of 30 s. The file is named $acDD\_HH\_MM.pas$. Here pairs of figures DD, HH, and MM specify the numbers Day, $Hour$ and $Minute$, which are indicated in the first line of the file: $DD = 14$ for September 14, $DD = 15$ for September 15, etc.

Figs. 1 — 4 illustrate the data contained in some files and the accuracy of approximation of the magnetic measurements, which was achieved in their processing. Each figure illustrate the data in two neighbor (by time) files. The plots in Figs. 1a, ..., 4a illustrate the accuracy of approximation of pseudo-measurements by the functions $h_i^\circ(t)$ defined in (3). Here, solid lines present plots of these functions in the proper interval $t_0 \le t \le t_0 + T$; marks indicate the points $\bigl(t_n, h_i^{(n)} - \Delta_i\bigr)$, $n = 0, 1, \ldots, N$. At that the left hand and right hand plots refer to separate files. The other plots in figures refer to both files simultaneously. Figs. 1b, ..., 4b illustrate the angular rates $\omega_i(t)$. Here, the left plots give general view of these functions, the right plots show the data at the interfaces between files in a large scale. The discrepancy between the data of neighbor files are coordinated well with the standard deviations of motion parameters obtained in [2]. Figs. 1c, ..., 4c illustrate in the same manner the angular accelerations $\dot\omega_i(t)$. Figs. 1d, ..., 4d and 1e, ..., 4e show plots of the functions e_i and b_{ai} respectively. There is no need to present the plots of the function $\chi(t)$ because it doesn't depend on spacecraft attitude motion.

Some comments to the figures. Figs. 2a and 4a illustrate approximation of pseudo-measurements that are defined on not uniform grids. Intervals 32 and 56, showed there, have lacks of some grid points in their middle parts. These lacks are caused by gaps in the measurement data. Fig. 3b illustrates the jump of the angular rate ω_1 caused by turning off the BIOBOX centrifuge. This turning off took place near the end of interval 40. Table 1 contains the estimates of the parameter q_1, which depends additively on the own centrifuge angular momentum. These estimates have a jump in transition from interval; 40 interval 41 (see the table), which corresponds to turning off the BIOBOX centrifuge.

Figs 1f, ..., 4f illustrate the acceleration $\mathbf{b} = (b_1, b_2, b_3)$ calculated by formula (1) using the data obtained. All calculations were made for the points $P = (-1\text{m}, -0.9\text{m}, 0.2\text{m})$. Each figure illustrates the data in two neighbor files. Here, the left plots give a general view of the functions b_i, the right plots show the same functions at the interfaces between files in a large scale. The discrepancy between the functions of neighbor files are adjusted sufficiently well. If there is a need for a smooth coupling of functions corresponding to neighbor files, then usual smoothing procedures can be used. Fig. 3g gives the example of such smooth coupling. We used here the following procedure. Let we have the functions $b'_i(t)$ and $b''_i(t)$ defined respectively in the intervals $t \le t'$ and $t'' \le t$, where $t'' < t'$. We put $b_i(t) = b'_i(t)$ when $t \le t''$, $b_i(t) = b''_i(t)$ when $t \ge t'$, and

$$b_i(t) = c(t)b'_i(t) + [1 - c(t)]b''_i(t), \quad c(t) = \frac{1}{2}\left[1 + \cos\frac{\pi(t - t'')}{t' - t''}\right]$$

when $t' < t < t''$. This procedure can be used for smooth coupling the functions $\omega_i(t)$, $e_i(t)$, etc., if this needs.

This work was partly supported by Russian Foundation for Basic Research (project 08-01-00467).

References

[1] Sazonov V.V., Komarov M.M., Polezhaev V.I., Nikitin S.A., Ermakov M.K., Stazhkov V.M., Zykov S.G., Ryabukha S.B., Acevedo J., Liberman E. Microaccelerations on board the Mir orbital station and prompt analysis of gravitational sensitivity of convective processes of heat and mass transfer. Cosmic Research, 1999, vol. 37, No. 1, pp. 80-94.

[2] Beuselinck T., Van Bavinchove C., Abrashkin V.I., Kazakova A.E., Sazonov V.V. Determination of the spacecraft *Foton M-3* attitude motion on measurements of the Earth magnetic field. Preprints of the Keldysh Institute of Applied Mathematics, No. 80, 2008.

[3] GOST R (State standard) 25645.166-2004. Earth upper atmosphere. Density model for ballistic support of flights of artificial Earth satellites. Moscow, 2004.

Table 1. Basic characteristics of the processed intervals

Int. No.	Date 09.07	t_0 (UTC), h:m:s	N	File of results	s_H, g	q_1, $10^{-3}\,s^{-1}$	s_{q1}, $10^{-3}\,s^{-1}$
1	14	13:55:34	150	Ac14_13_55	803	0.9108	0.024
2	14	16:15:36	150	ac14_16_15	928	0.8523	0.015
3	14	18:35:33	150	ac14_18_35	800	0.8902	0.011
4	14	20:55:45	150	ac14_20_55	681	0.7749	0.012
5	14	23:15:34	210	ac14_23_15	683	0.8844	0.0069
6	15	02:35:34	210	ac15_02_35	928	0.7808	0.014
7	15	05:55:34	210	ac15_05_55	1291	0.7206	0.017
8	15	09:15:33	210	ac15_09_15	837	0.7598	0.011
9	15	12:35:36	210	ac15_12_35	792	0.7066	0.014
10	15	15:55:32	210	ac15_15_55	1133	1.0714	0.015
11	15	19:15:38	180	ac15_19_15	762	0.9509	0.0097
12	15	22:05:41	180	ac15_22_05	950	0.8607	0.013
13	16	00:55:42	150	ac16_00_55	1290	0.8762	0.022
14	16	03:15:53	180	ac16_03_15	899	0.9544	0.013
15	16	06:06:04	180	ac16_06_06	1024	0.9193	0.015
16	16	08:56:03	240	Ac16_08_56	964	0.8240	0.013
17	16	12:46:10	180	Ac16_12_46	1264	0.9075	0.020
18	16	15:36:06	210	Ac16_15_36	720	0.9001	0.0098
19	16	18:56:03	150	ac16_18_56	844	0.9029	0.018
20	16	21:16:03	120	ac16_21_16	724	0.8675	0.017
21	16	23:06:07	120	ac16_23_06	985	0.7397	0.024
22	17	00:56:06	180	ac17_00_56	1008	0.8678	0.0026
23	17	03:46:07	120	ac17_03_46	809	0.8251	0.017
24	17	05:36:07	120	ac17_05_36	749	0.8086	0.026
25	17	07:26:07	240	Ac17_07_26	972	0.6030	0.018
26	17	11:16:03	240	Ac17_11_56	811	0.7291	0.014
27	17	15:06:06	240	Ac17_15_06	1083	0.6889	0.016
28	17	18:56:03	240	Ac17_18_56	935	0.6591	0.015

Table 1 (continuation). Basic characteristics of the processed intervals

Int. No.	Date 09.07	t_0 (UTC), h:m:s	N	File of results	s_H, g	q_1, $10^{-3}\,s^{-1}$	s_{q1}, $10^{-3}\,s^{-1}$
29	17	22:46:02	240	Ac17_22_46	966	0.6933	0.016
30	18	02:36:00	240	Ac18_02_36	1112	0.7392	0.023
31	18	06:26:08	360	ac18_06_26	812	0.6952	0.012
32	18	12:16:10	720	ac18_12_16	844	0.5754	0.0086
33	18	18:06:07	360	ac18_18_06	1152	0.5470	0.015
34	18	23:56:18	360	ac18_23_56	1054	0.6364	0.013
35	19	05:46:24	360	ac19_05_46	791	0.5552	0.0098
36	19	11:36:18	360	ac19_11_36	655	0.5265	0.0093
37	19	17:26:19	360	ac19_17_26	726	0.4208	0.0078
38	19	23:16:23	270	ac19_23_16	768	0.4813	0.013
39	20	03:36:25	270	ac20_03_36	903	0.4574	0.015
40	20	07:56:33	210	ac20_07_56	693	0.4745	0.014
41	20	11:16:35	360	ac20_11_16	803	0.1661	0.010
42	20	17:06:44	360	ac20_17_06	678	0.1970	0.0079
43	20	22:56:44	360	ac20_22_56	654	0.1402	0.0081
44	21	04:47:00	360	ac21_04_47	569	0.1648	0.0082
45	21	10:36:57	360	ac21_10_36	859	0.0825	0.012
46	21	16:26:59	360	ac21_16_26	668	0.0776	0.0091
47	21	22:17:03	360	ac21_22_17	625	0.1359	0.0081
48	22	04:07:01	360	ac22_04_07	738	0.1510	0.011
49	22	09:57:03	360	ac22_09_57	566	0.0818	0.0080
50	23	03:39:03	360	ac23_03_39	831	0.0552	0.013
51	23	09:29:04	360	ac23_09_29	628	0.1206	0.0081
52	23	15:19:07	360	ac23_15_19	842	0.0420	0.0085
53	23	21:09:07	360	ac23_21_09	690	0.0512	0.0075
54	24	02:59:12	360	ac24_02_59	889	0.0293	0.0093
55	24	05:25:10	421	ac24_05_25	869	0.0549	0.0082
56	24	09:37:14	337	Ac24_09_37	793	0.0049	0.0071
57	24	17:02:25	490	Ac24_17_02	728	0.0139	0.0040

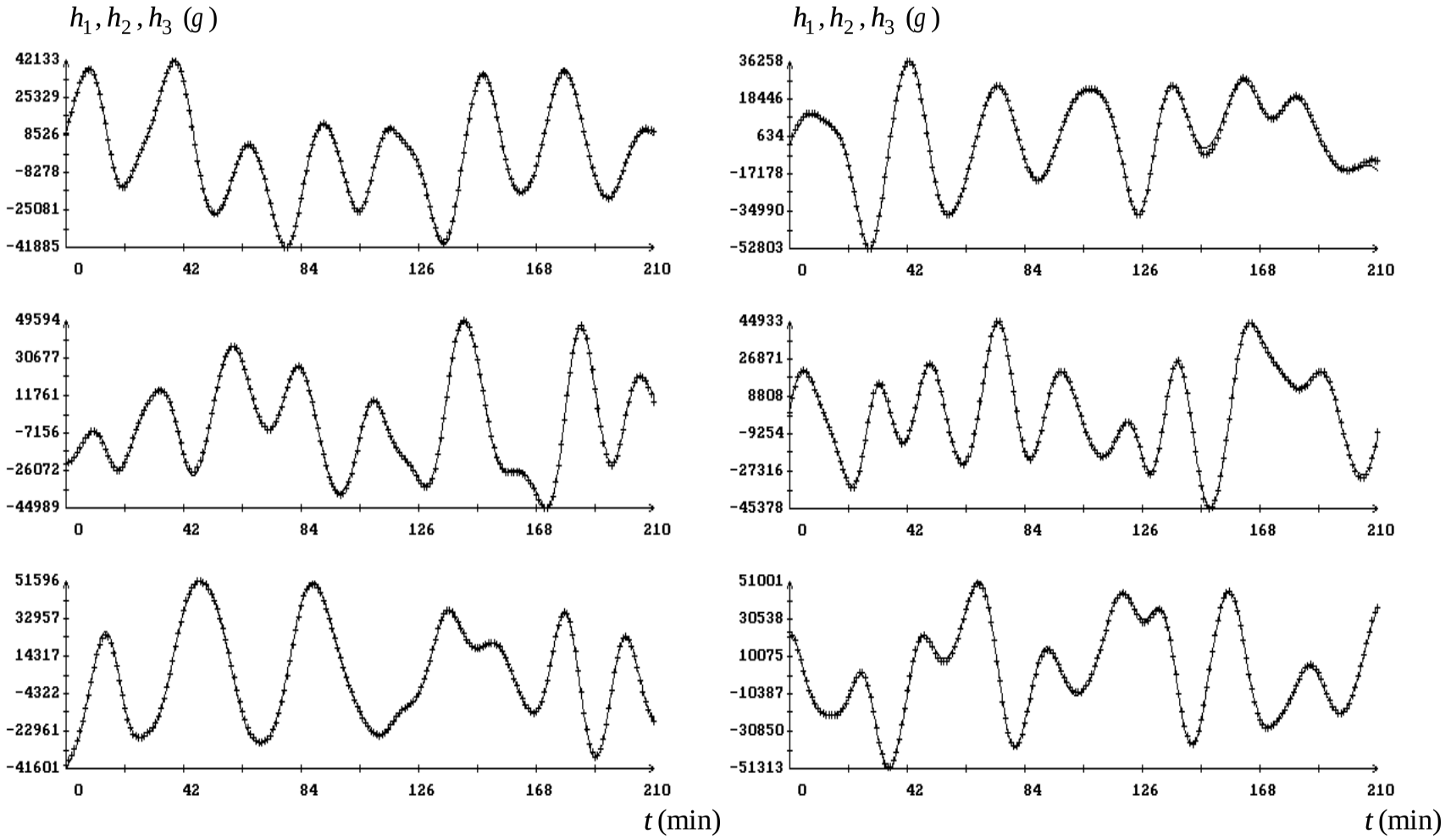

Fig. 1a. Approximation of magnetic pseudo-measurements by solutions of equations (2). On the left: the data from the file ac14_23_15.pas; the instant $t = 0$ in the plots corresponds to 23:15:34 UTC 14.09.2007. On the right: the data from the file ac15_02_35.pas; the instant $t = 0$ in the plots corresponds to 02:35:34 UTC 15.09.2007.

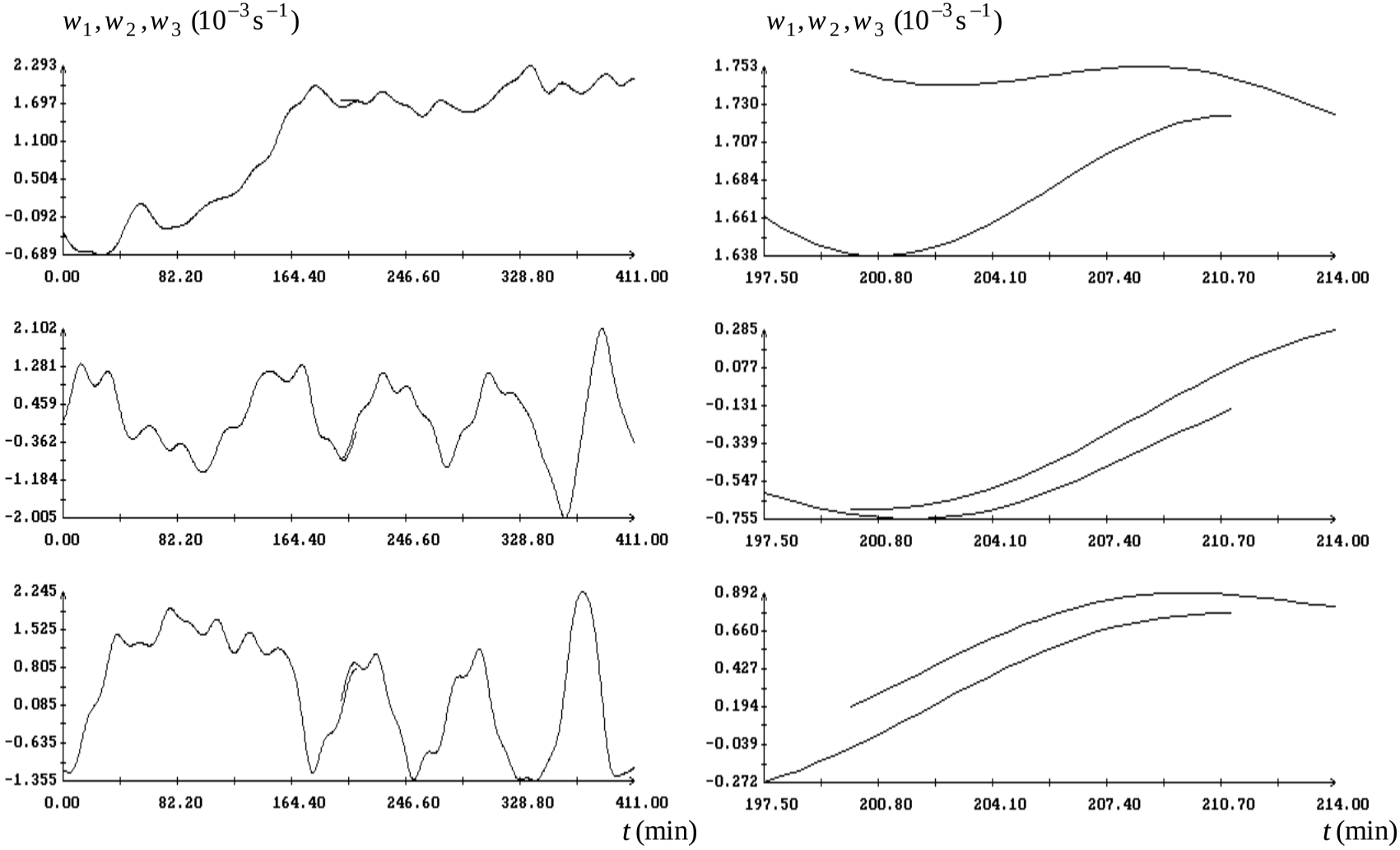

Fig. 1b. Mating of the data from the files ac14_23_15.pas and ac15_02_35.pas. The components of the angular rate. The instant $t = 0$ in the plots corresponds to 23:15:34 UTC 14.09.2007.

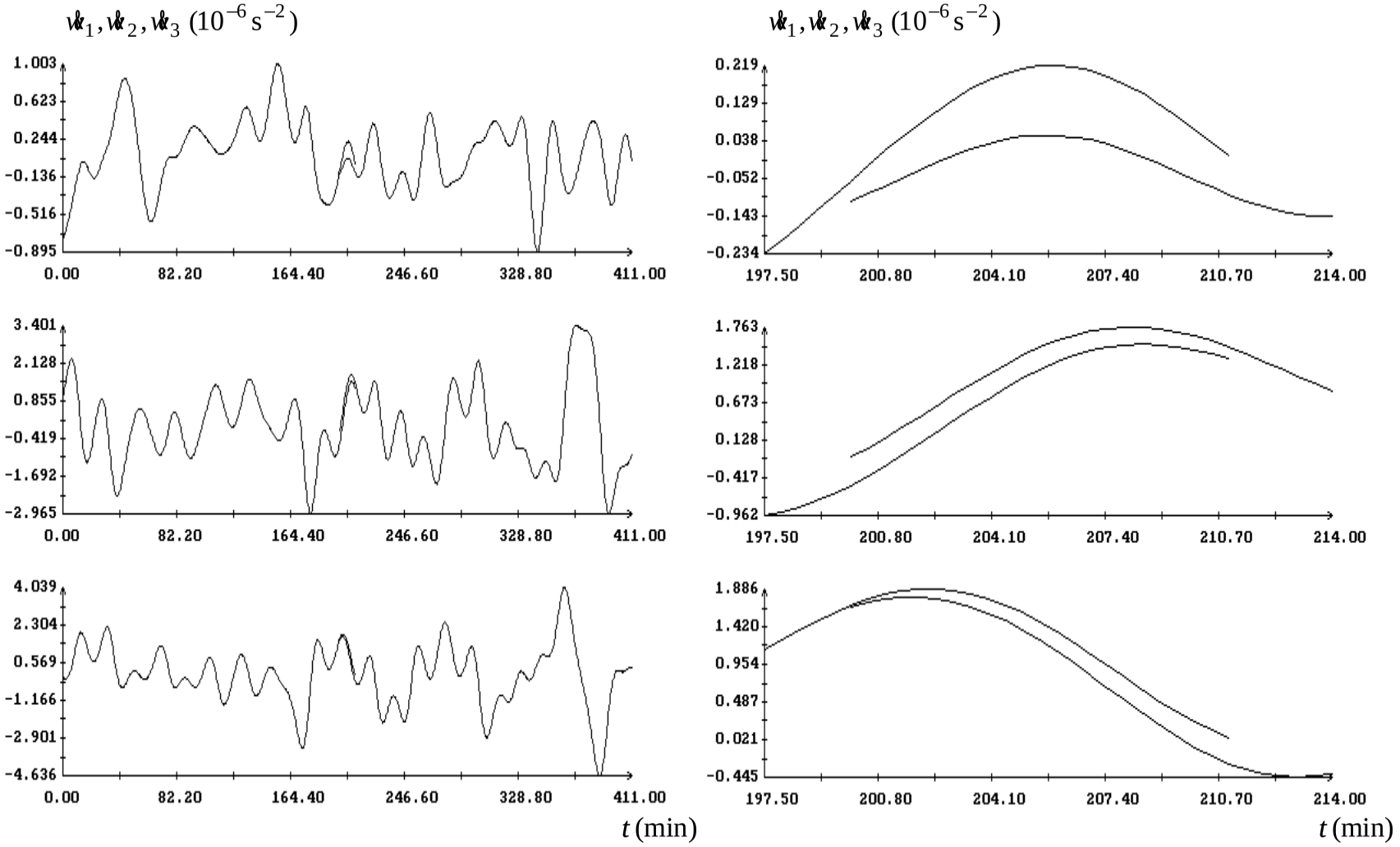

Fig. 1c. Mating of the data from the files ac14_23_15.pas and ac15_02_35.pas. The components of the angular acceleration. The instant $t = 0$ in the plots corresponds to 23:15:34 UTC 14.09.2007.

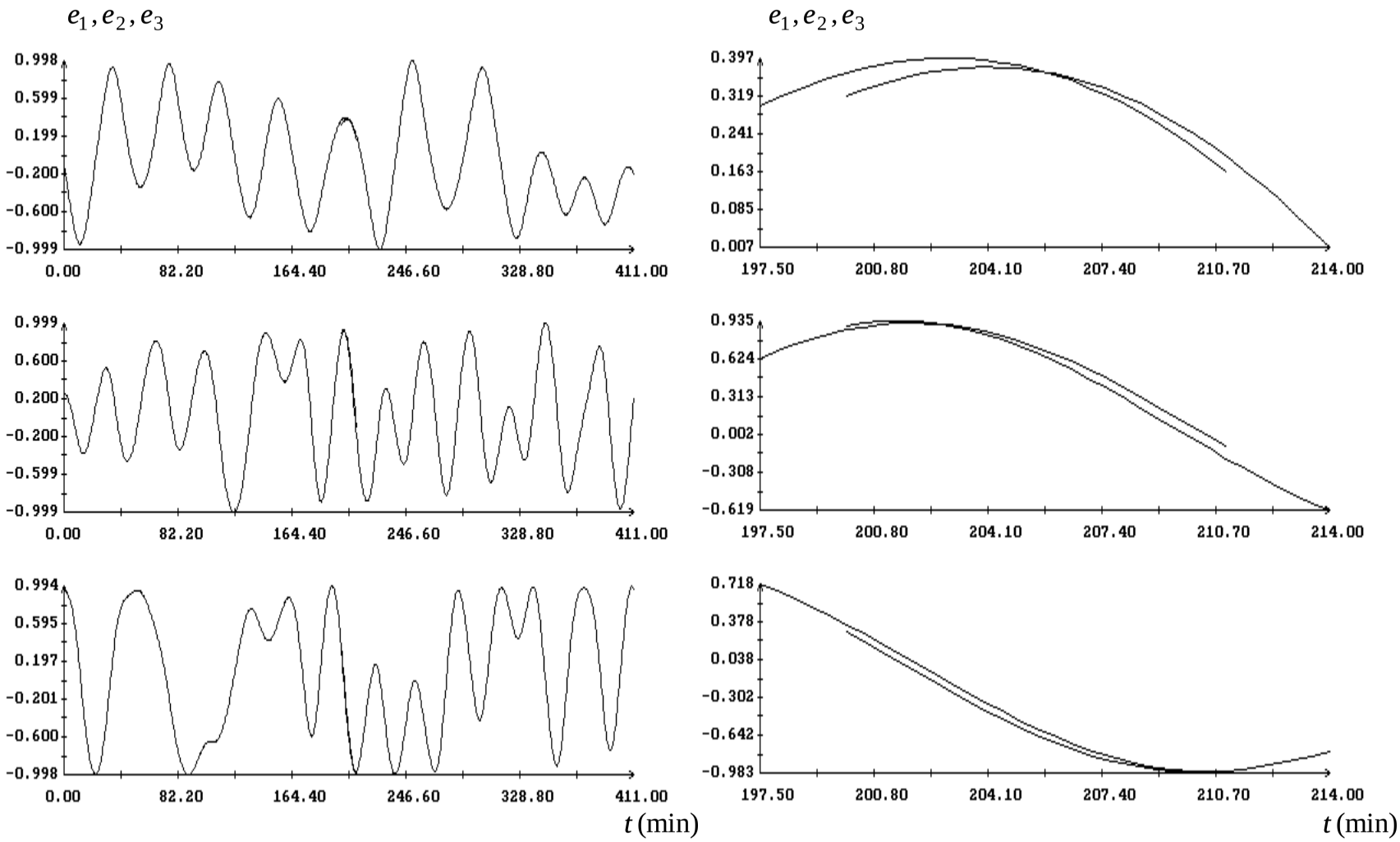

Fig. 1d. Mating of the data from the files ac14_23_15.pas and ac15_02_35.pas. The components of the unit vector $\mathbf{e} = \mathbf{R} / |\mathbf{R}|$. The instant $t = 0$ in the plots corresponds to 23:15:34 UTC 14.09.2007.

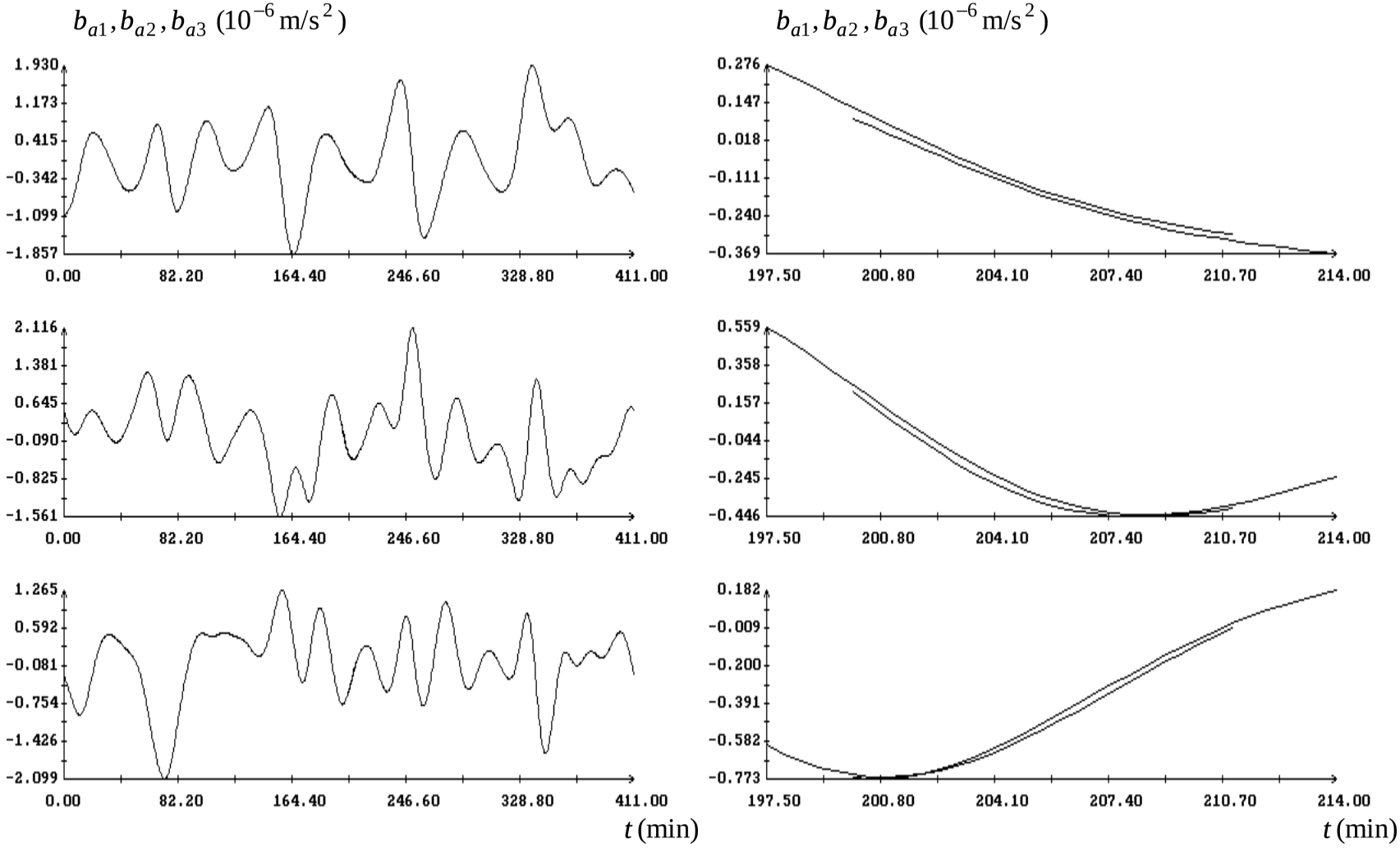

Fig. 1e. Mating of data from the files ac14_23_15.pas and ac15_02_35.pas. The components of the aerodynamic part of the acceleration. The instant $t = 0$ in the plots corresponds to 23:15:34 UTC 14.09.2007.

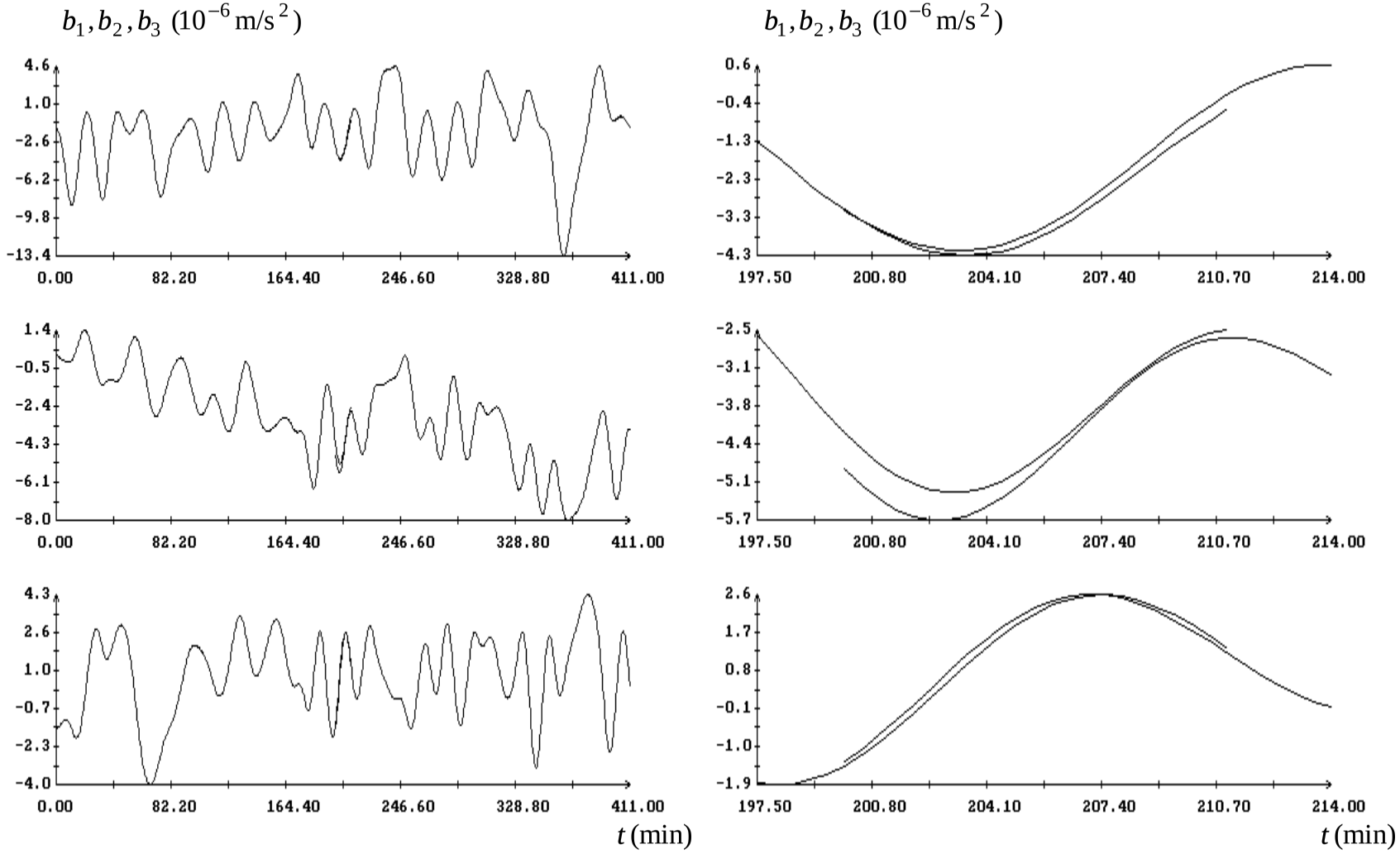

Fig. 1f. Mating of the data from the files ac14_23_15.pas and ac15_02_35.pas. The components of the acceleration at the point $P = (-1\text{m}, -0.9\text{m}, 0.2\text{m})$. The instant $t = 0$ in the plots corresponds to 23:15:34 UTC 14.09.2007.

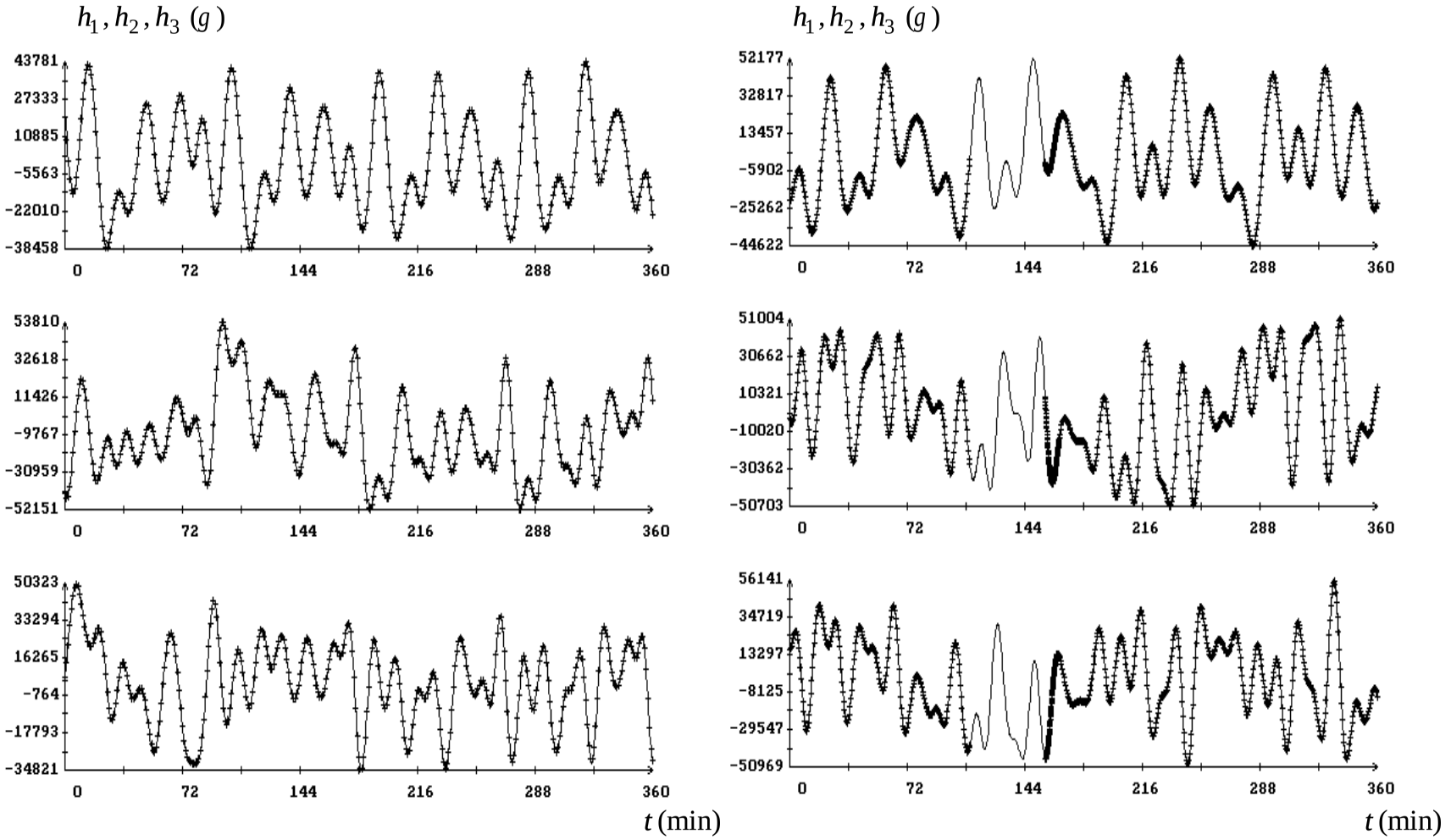

Fig. 2a. Approximation of magnetic pseudo-measurements by solutions of equations (2). On the left: the data from the file ac18_06_26.pas; the instant $t = 0$ in the plots corresponds to 06:26:08 UTC 18.09.2007. On the right: On the right: the data from the file ac18_12_16.pas; the instant $t = 0$ in the plots corresponds to 12:16:10 UTC 18.09.2007.

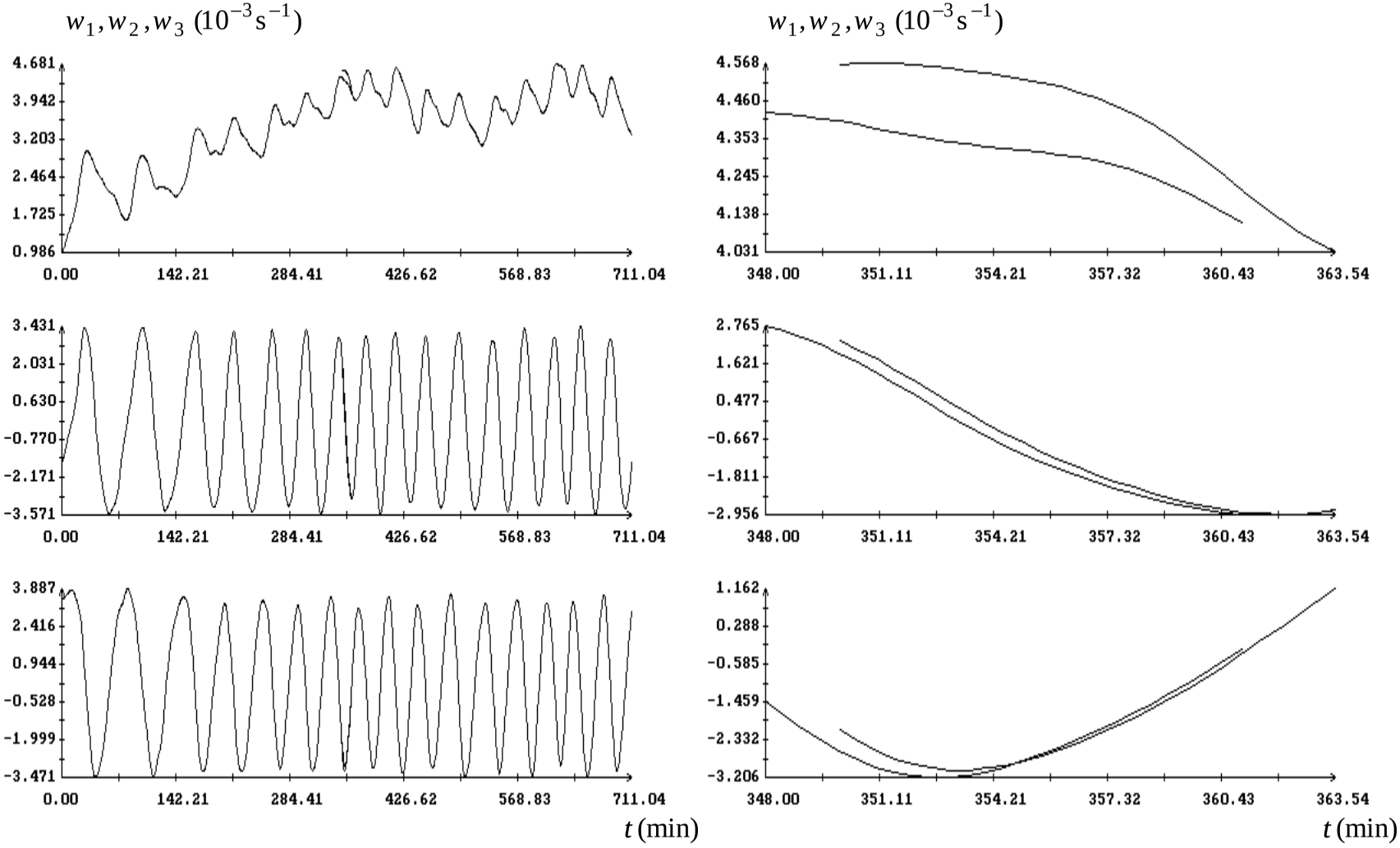

Fig. 2b. Mating of the data from the files ac18_06_26.pas and ac18_12_16.pas. The components of the angular rate. The instant $t = 0$ in the plots corresponds to 06:26:08 UTC 18.09.2007.

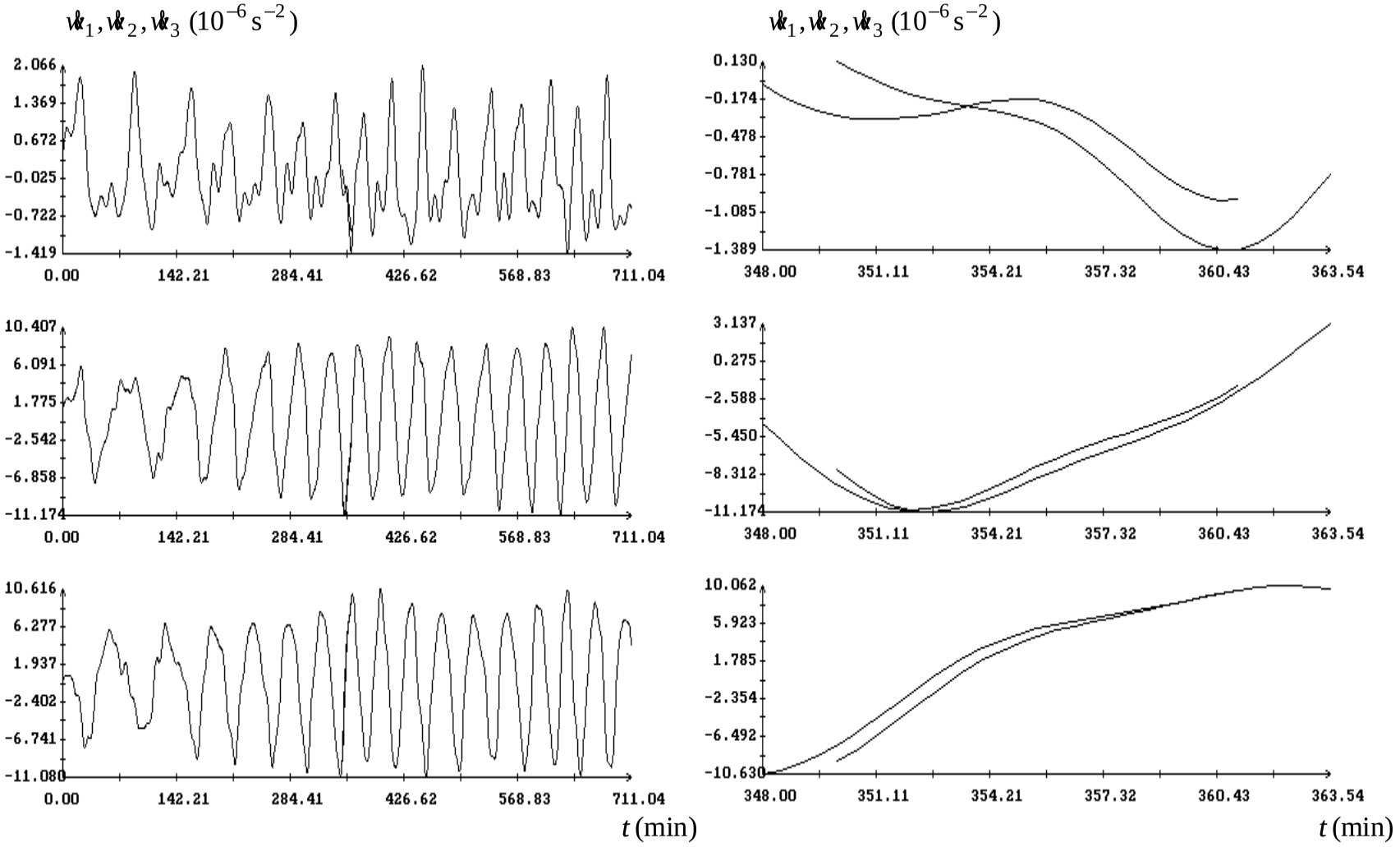

Fig. 2c. Mating of the data from the files ac18_06_26.pas and ac18_12_16.pas. The components of the angular acceleration. The instant $t = 0$ in the plots corresponds to 06:26:08 UTC 18.09.2007.

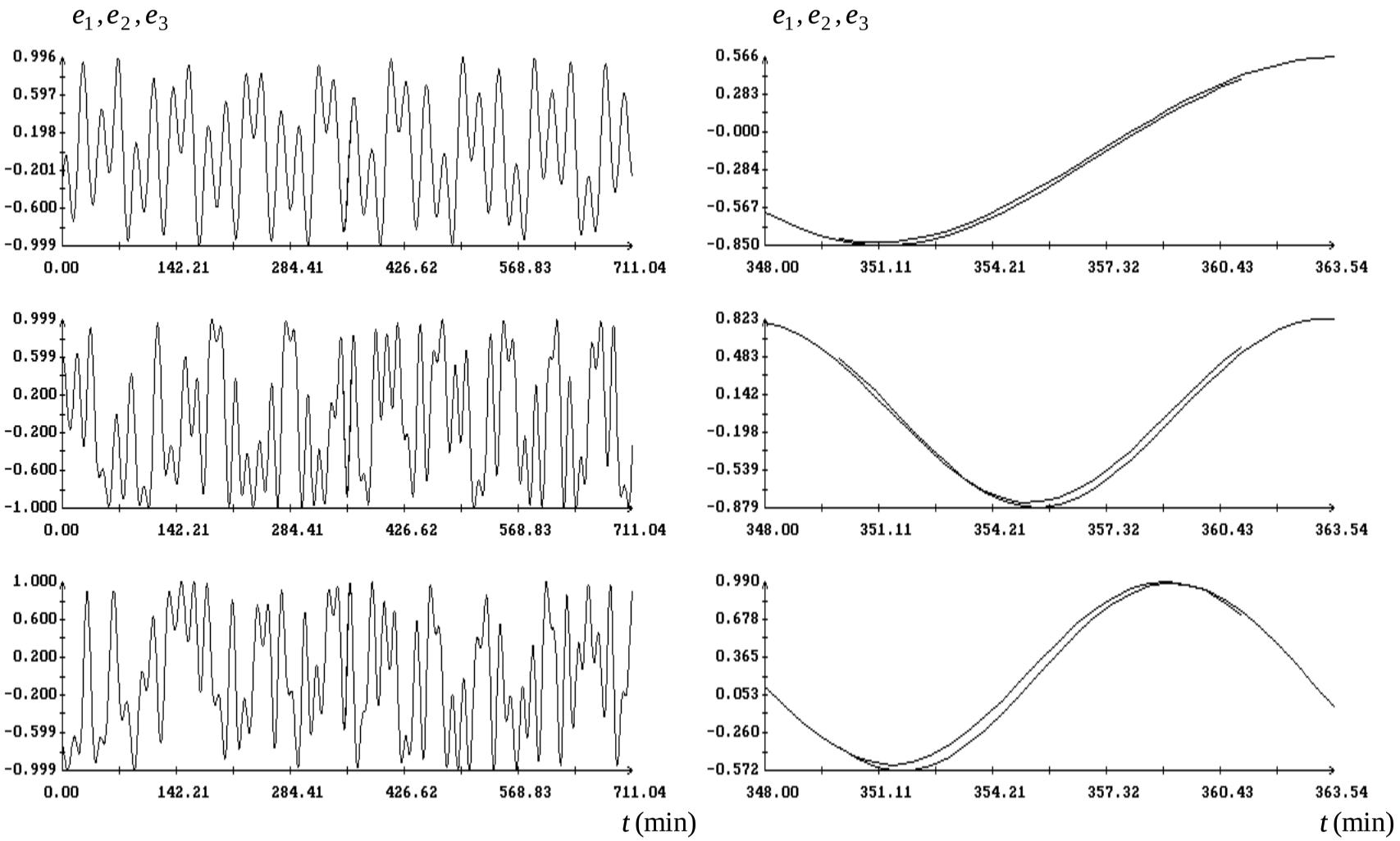

Fig. 2d. Mating of the data from the files ac18_06_26.pas and ac18_12_16.pas. The components of the unit vector $\mathbf{e} = \mathbf{R} / |\mathbf{R}|$. The instant $t = 0$ in the plots corresponds to 06:26:08 UTC 18.09.2007.

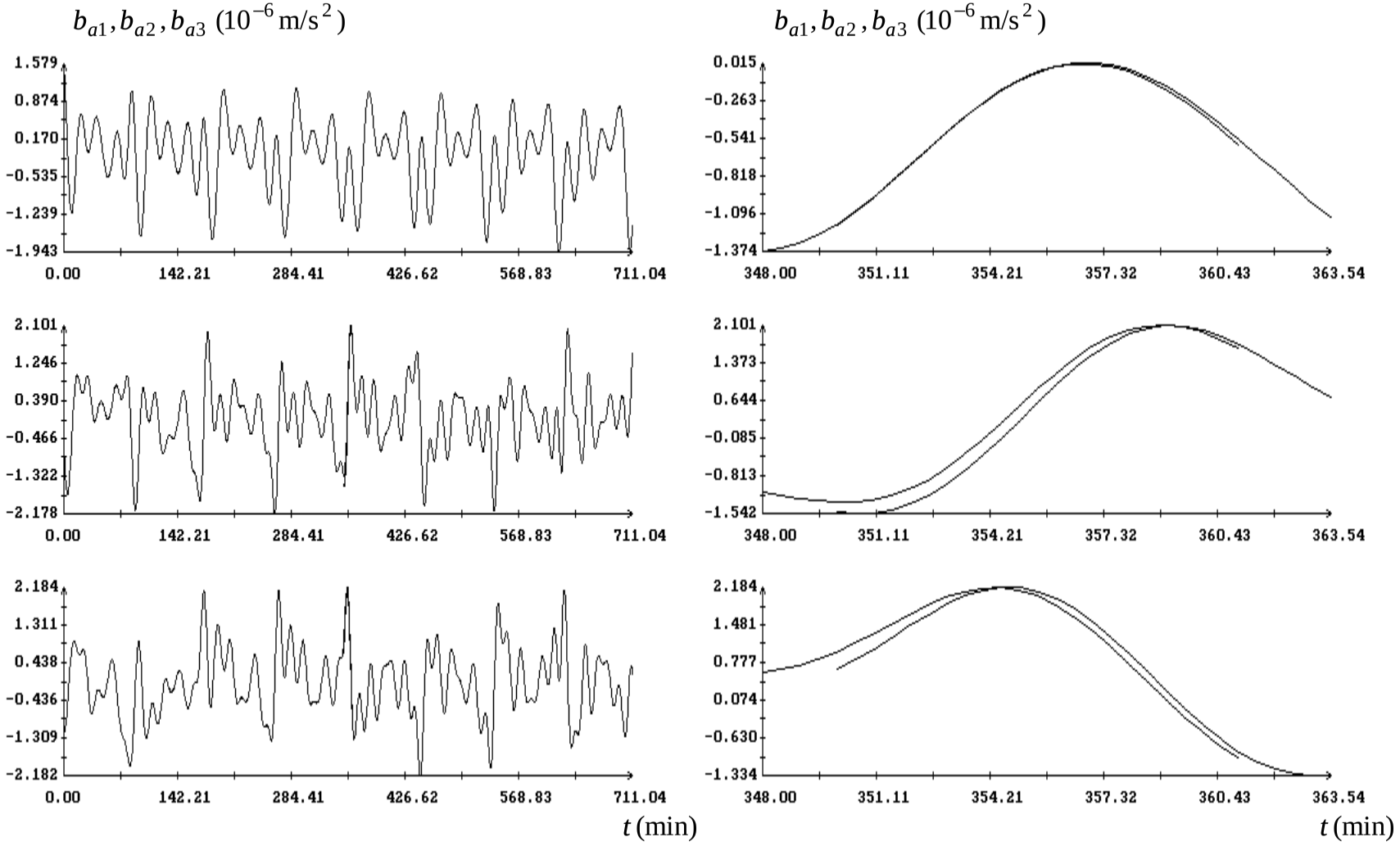

Fig. 2e. Mating of the data from the files ac18_06_26.pas and ac18_12_16.pas. The components of the aerodynamic part of the acceleration. The instant $t = 0$ in the plots corresponds to 06:26:08 UTC 18.09.2007.

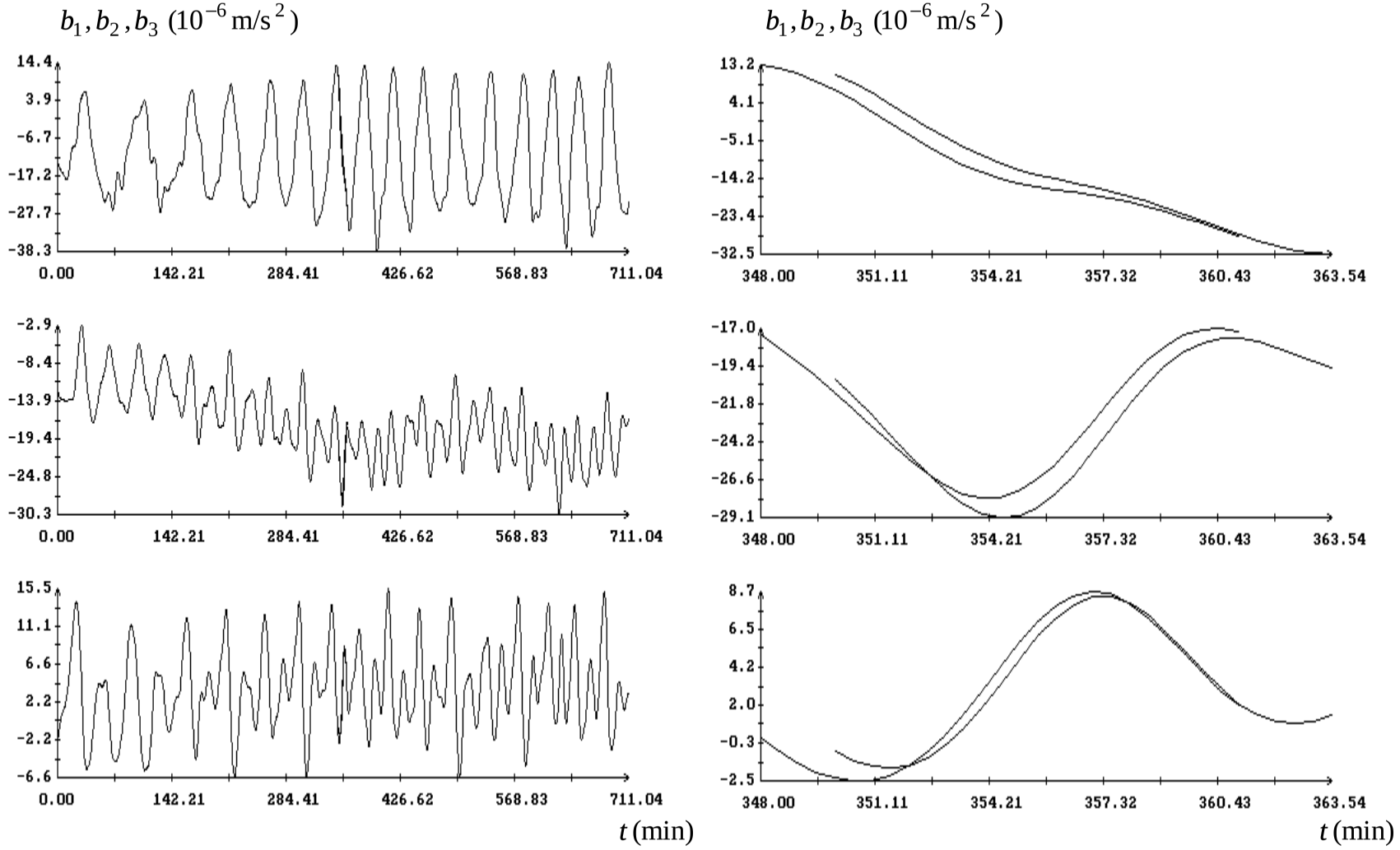

Fig. 2f. Mating of the data from the files ac18_06_26.pas and ac18_12_16.pas.pas. The components of the acceleration at the point $P = (-1\text{m}, -0.9\text{m}, 0.2\text{m})$. The instant $t = 0$ in the plots corresponds to 06:26:08 UTC 18.09.2007.

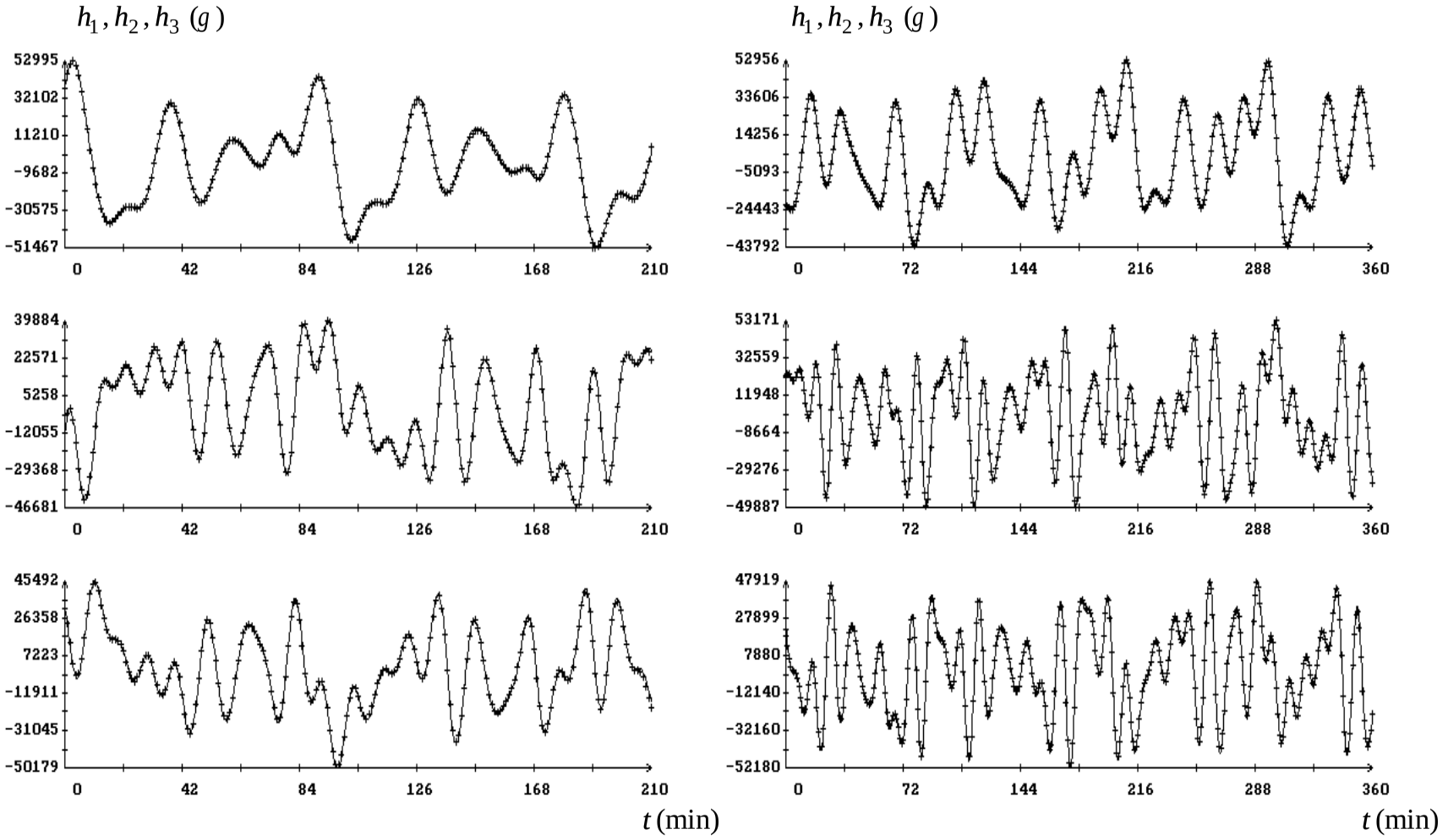

Fig. 3a. Approximation of magnetic pseudo-measurements by solutions of equations (2). On the left: the data from the file ac20_07_56.pas; the instant $t = 0$ in the plots corresponds to 07:56:33 UTC 20.09.2007. On the right: the data from the file ac20_11_16.pas; the instant $t = 0$ in the plots corresponds to 11:16:35 UTC 20.09.2007.

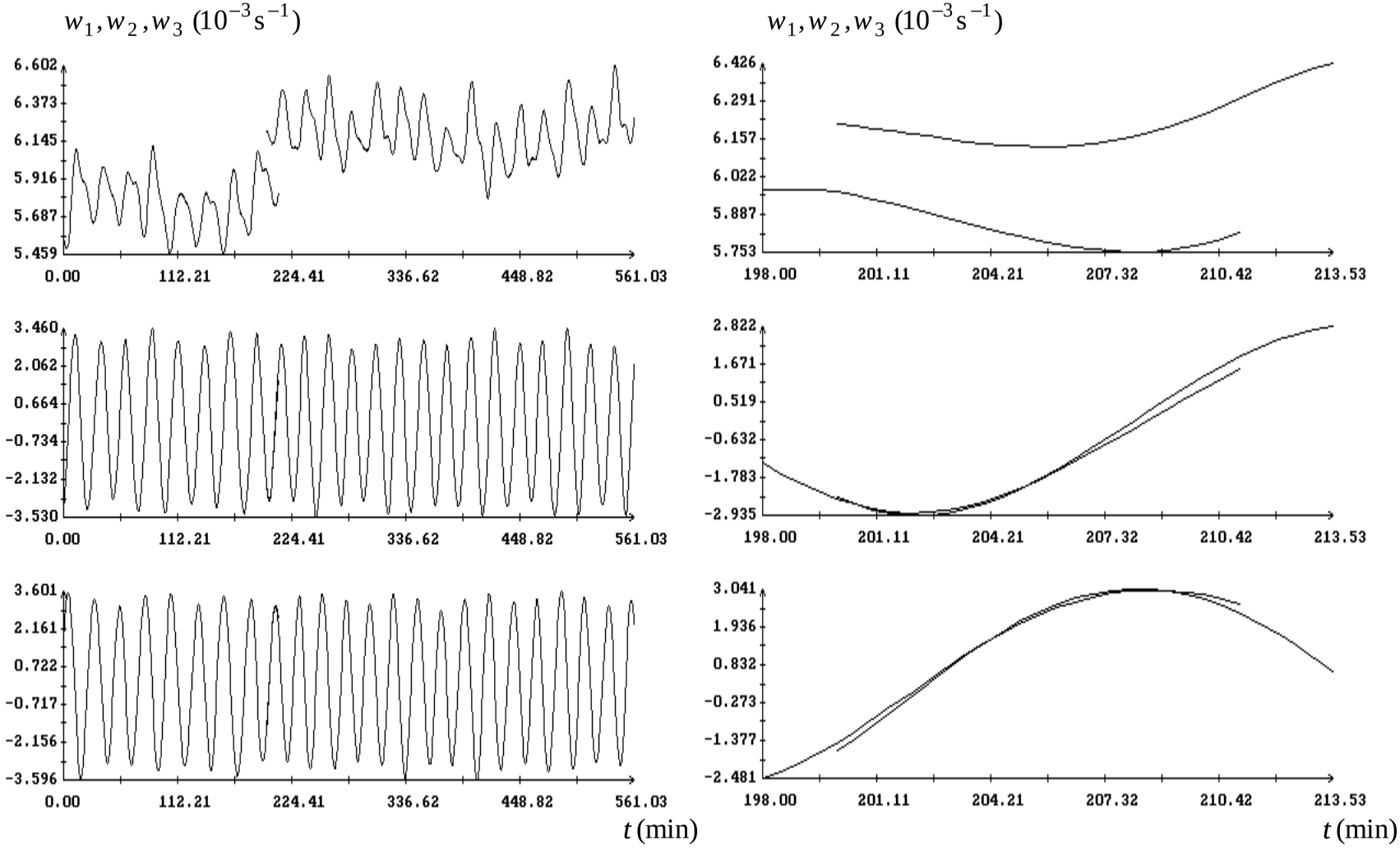

Fig. 3b. Mating of the data from the files ac20_07_56.pas and ac20_11_16.pas. The components of the angular rate. The instant $t = 0$ in the plots corresponds to 07:56:33 UTC 20.09.2007.

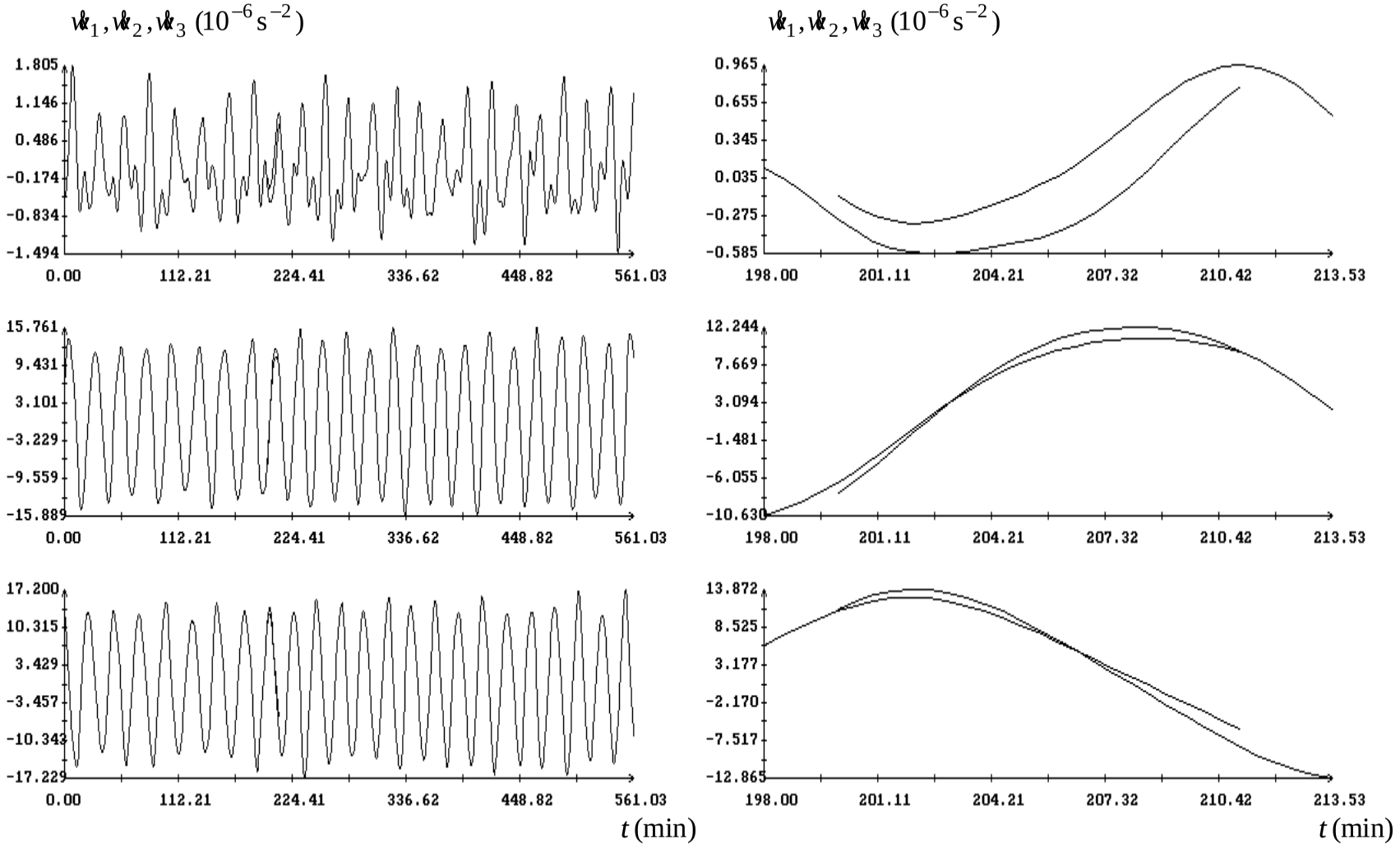

Fig. 3c. Mating of the data from the files ac20_07_56.pas and ac20_11_16.pas. The components of the angular acceleration. The instant $t = 0$ in the plots corresponds to 07:56:33 UTC 20.09.2007.

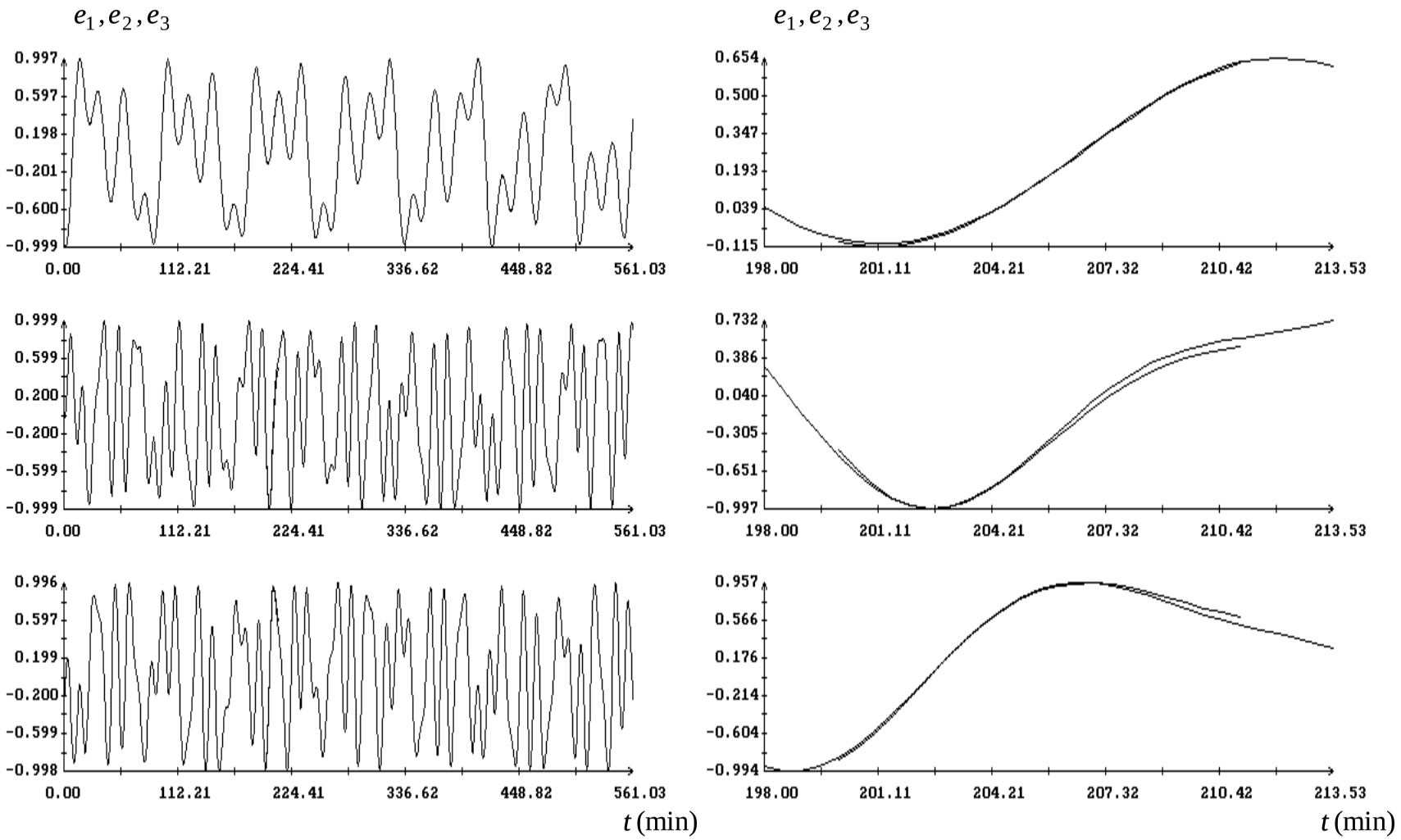

Fig. 3d. Mating of the data from the files ac20_07_56.pas and ac20_11_16.pas. The components of the unit vector $\mathbf{e} = \mathbf{R} / |\mathbf{R}|$. The instant $t = 0$ in the plots corresponds to 07:56:33 UTC 20.09.2007.

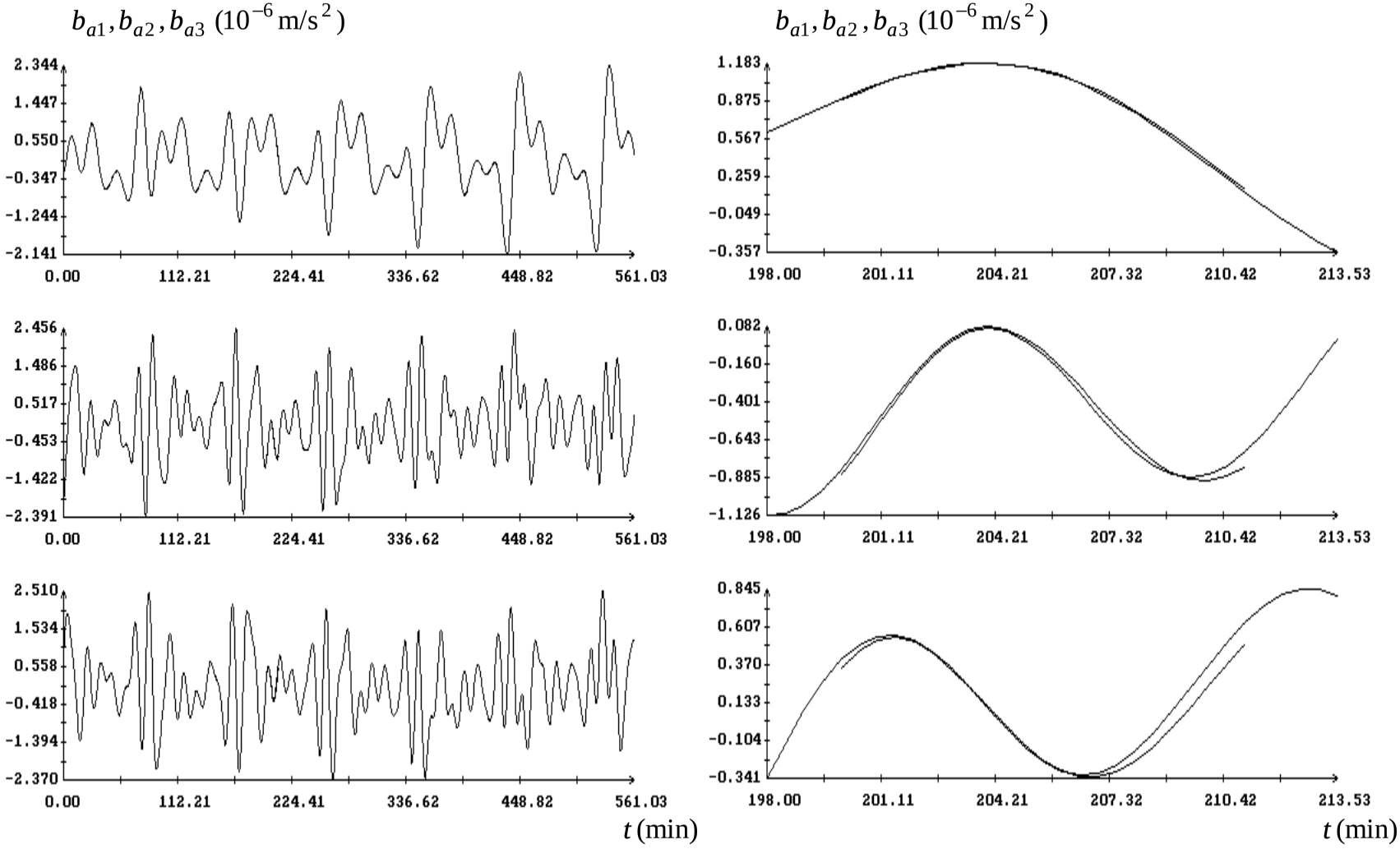

Fig. 3e. Mating of the data from the files ac20_07_56.pas and ac20_11_16.pas. The components of the aerodynamic part of the acceleration. The instant $t = 0$ in the plots corresponds to 07:56:33 UTC 20.09.2007.

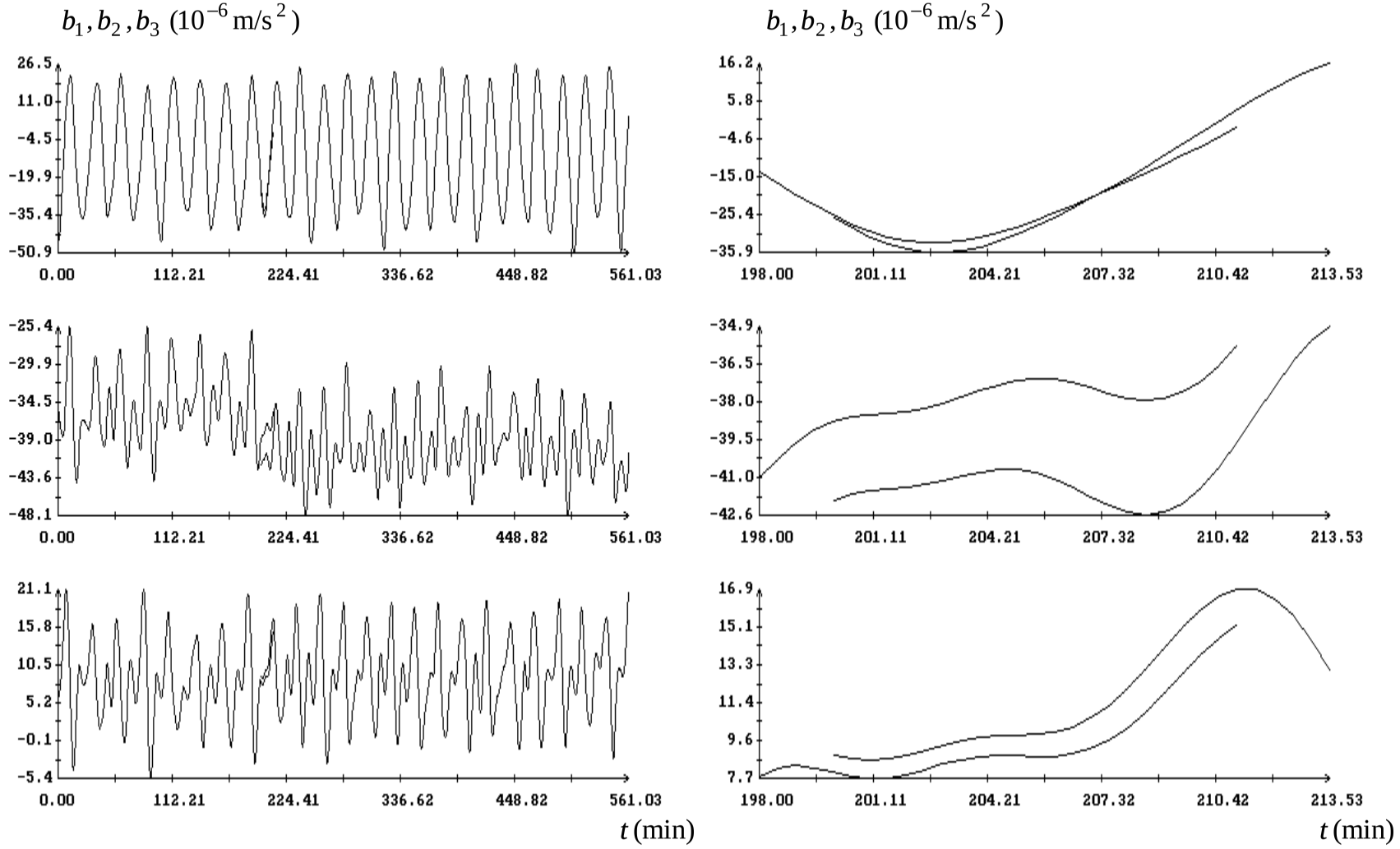

Fig. 3f. Mating of the data from the files ac20_07_56.pas and ac20_11_16.pas. The components of the acceleration at the point $P = (-1\text{m}, -0.9\text{m}, 0.2\text{m})$. The instant $t = 0$ in the plots corresponds to 07:56:33 UTC 20.09.2007.

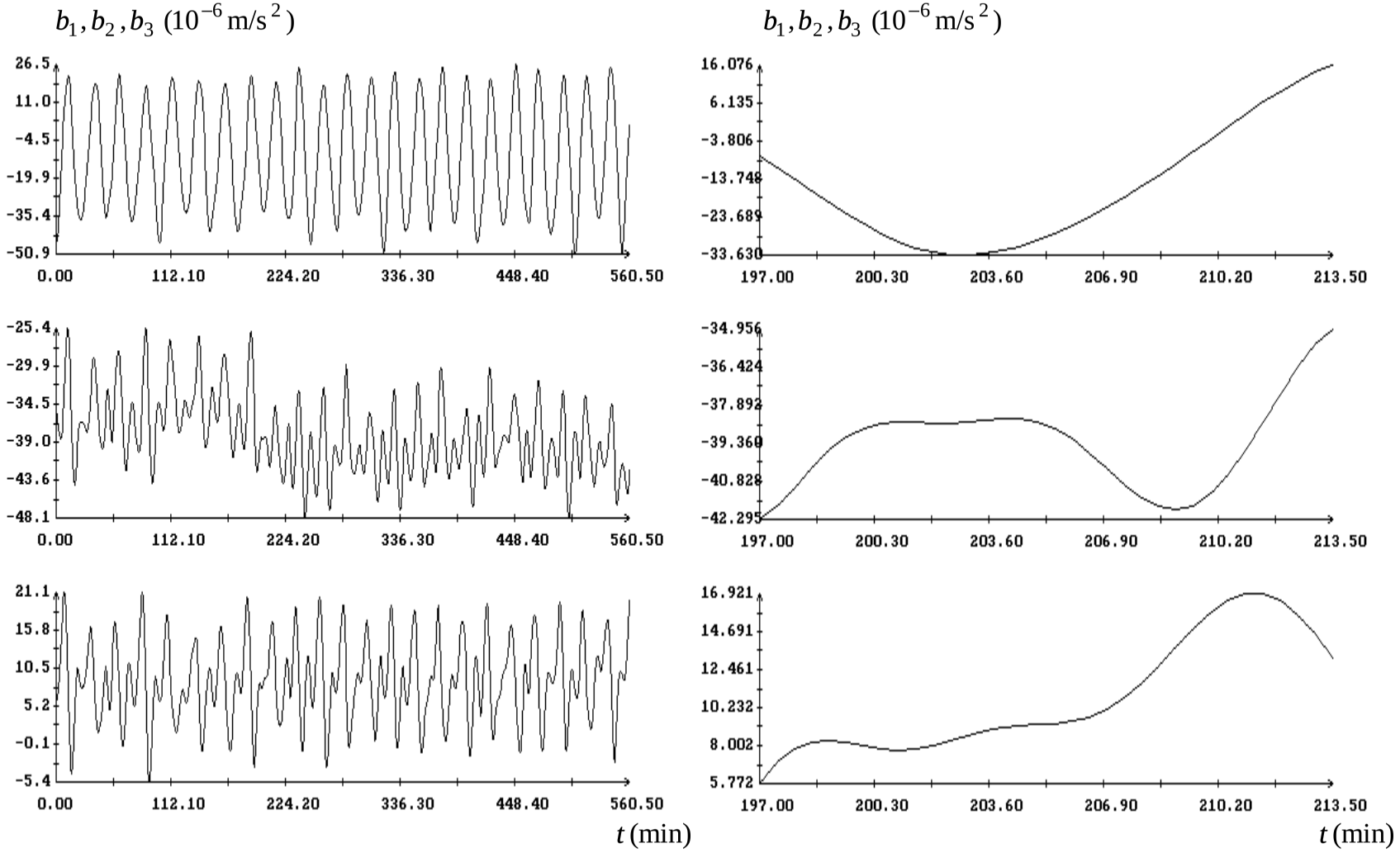

Fig. 3g. Smooth mating of the accelerations calculated by the data from the files ac20_07_56.pas and ac20_11_16.pas. The calculations were made for the point $P = (-1\text{m}, -0.9\text{m}, 0.2\text{m})$. The instant $t = 0$ corresponds to 07:56:33 UTC 20.09.2007.

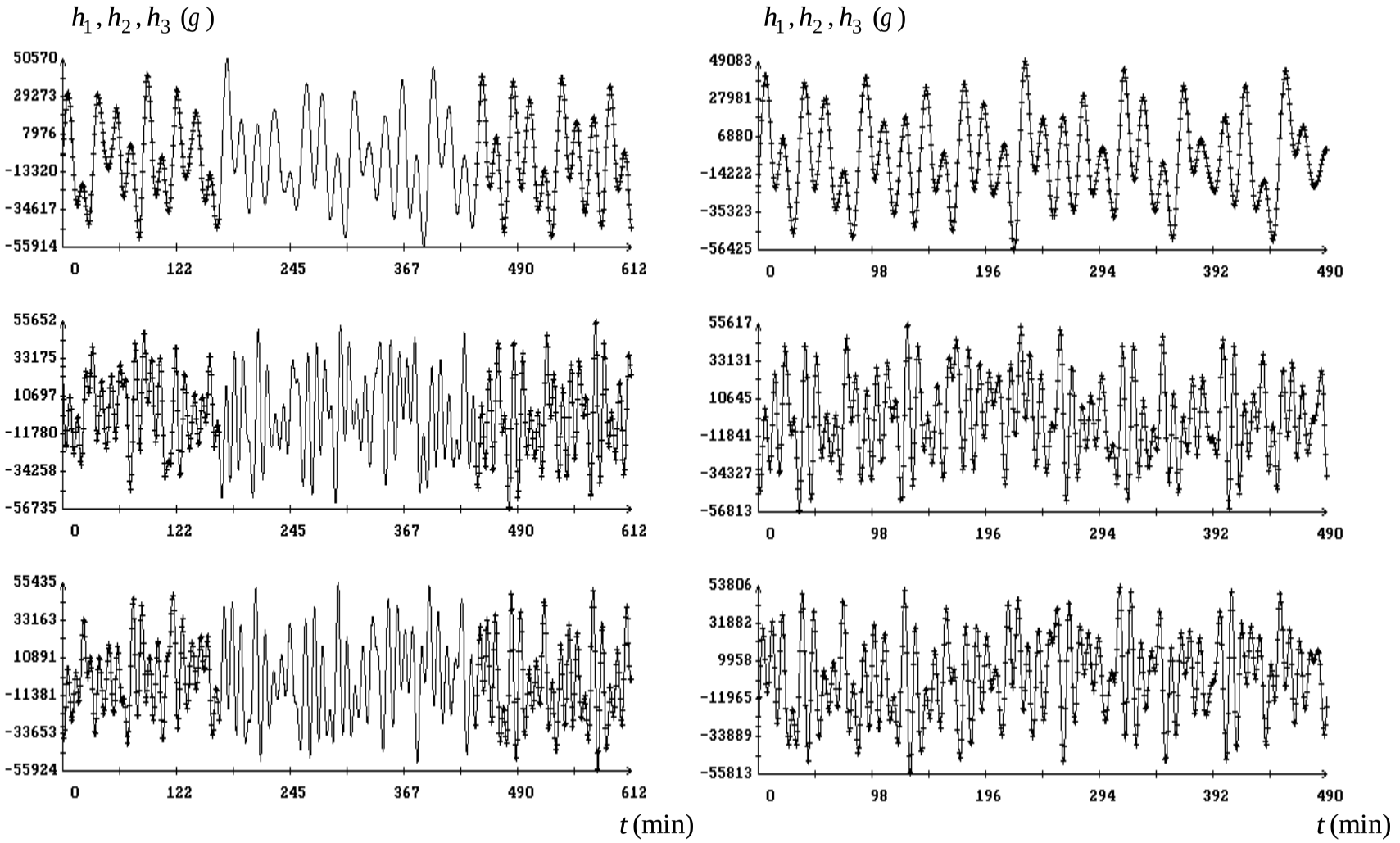

Fig. 4a. Approximation of magnetic pseudo-measurements by solutions of equations (2). On the left: the data from the file ac24_09_37.pas; the instant $t = 0$ in the plots corresponds to 09:37:14 UTC 24.09.2007. On the right: the data from the file ac24_17_02.pas; the instant $t = 0$ in the plots corresponds to 17:02:25 UTC 24.09.2007.

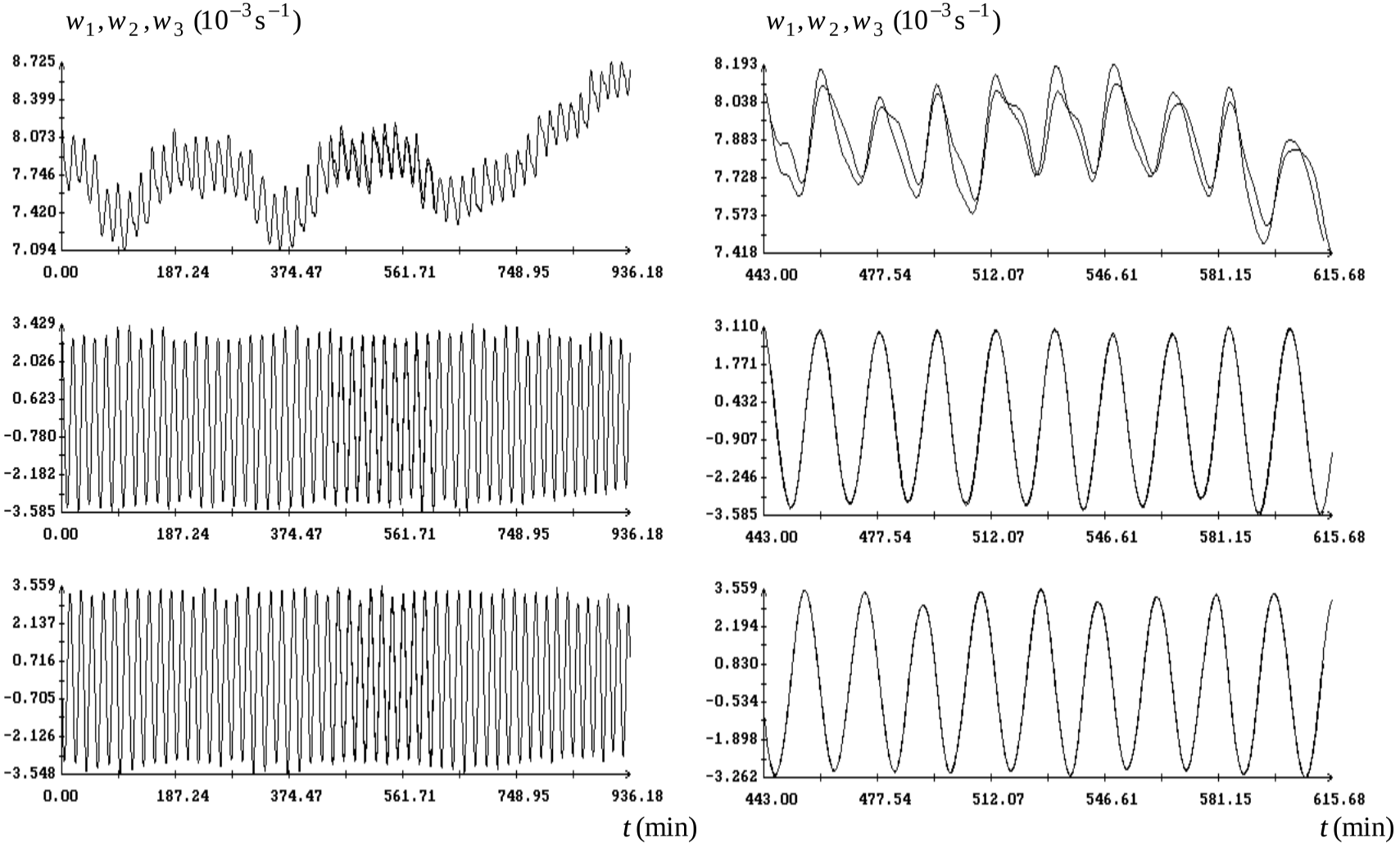

Fig. 4b. Mating of the data from the files ac24_09_37.pas and ac24_17_02.pas. The components of the angular rate. The instant $t = 0$ in the plots corresponds to 09:37:14 UTC 24.09.2007.

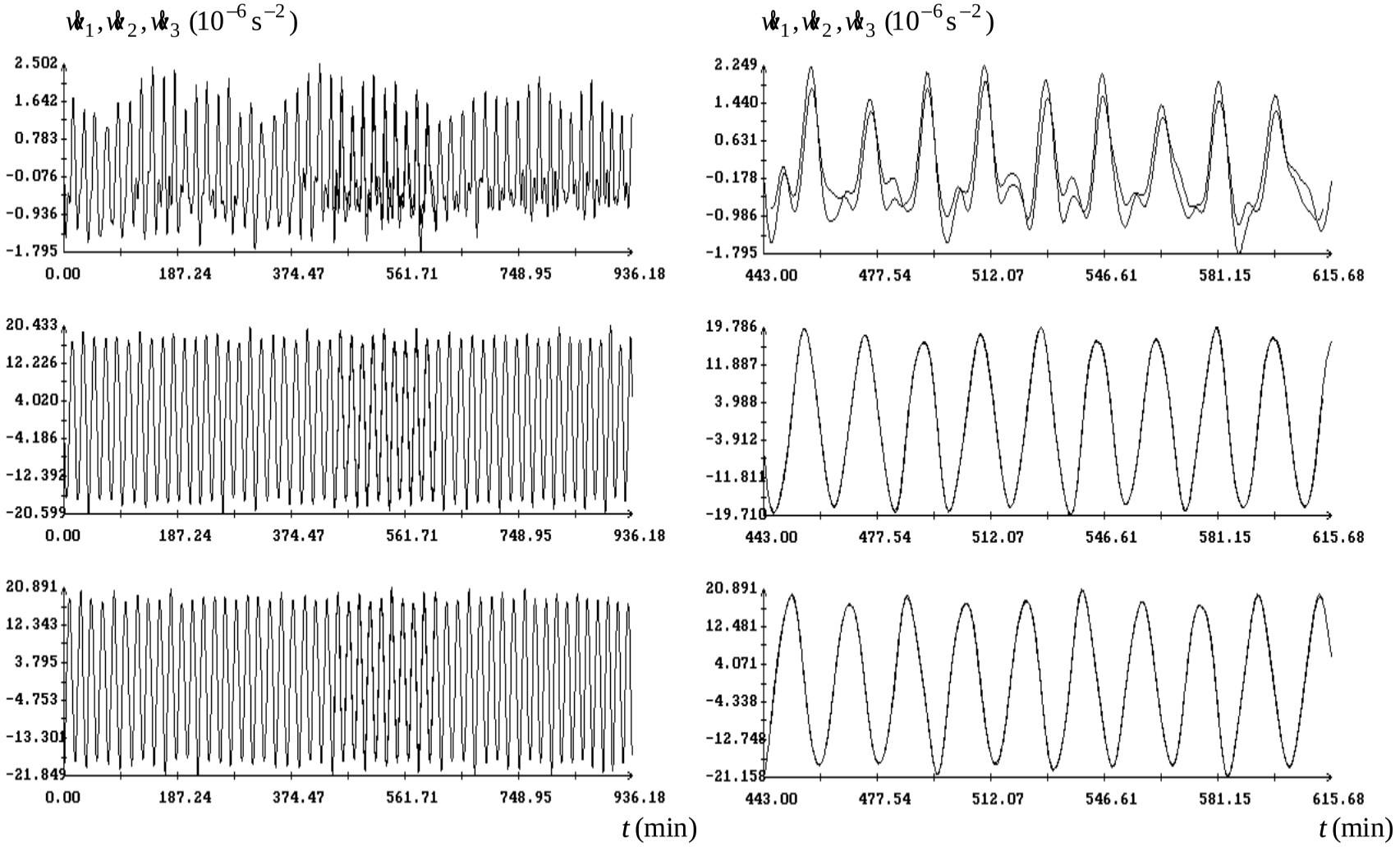

Fig. 4c. Mating of the data from the files ac24_09_37.pas and ac24_17_02.pas. The components of the angular acceleration. The instant $t = 0$ in the plots corresponds to 09:37:14 UTC 24.09.2007.

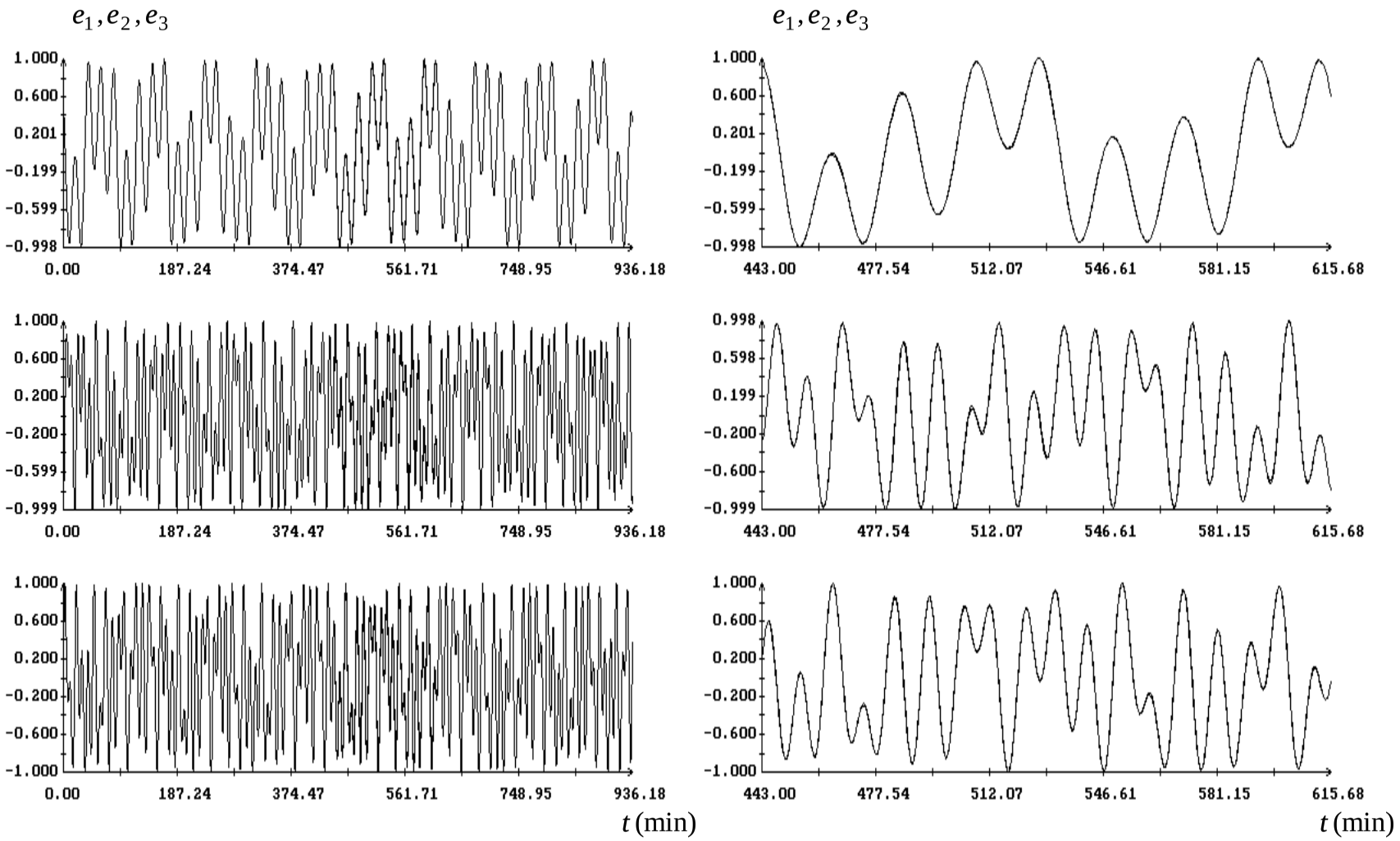

Fig. 4d. Mating of the data from the files ac24_09_37.pas and ac24_17_02.pas. The components of the unit vector $\mathbf{e} = \mathbf{R} / |\mathbf{R}|$. The instant $t = 0$ in the plots corresponds to 09:37:14 UTC 24.09.2007.

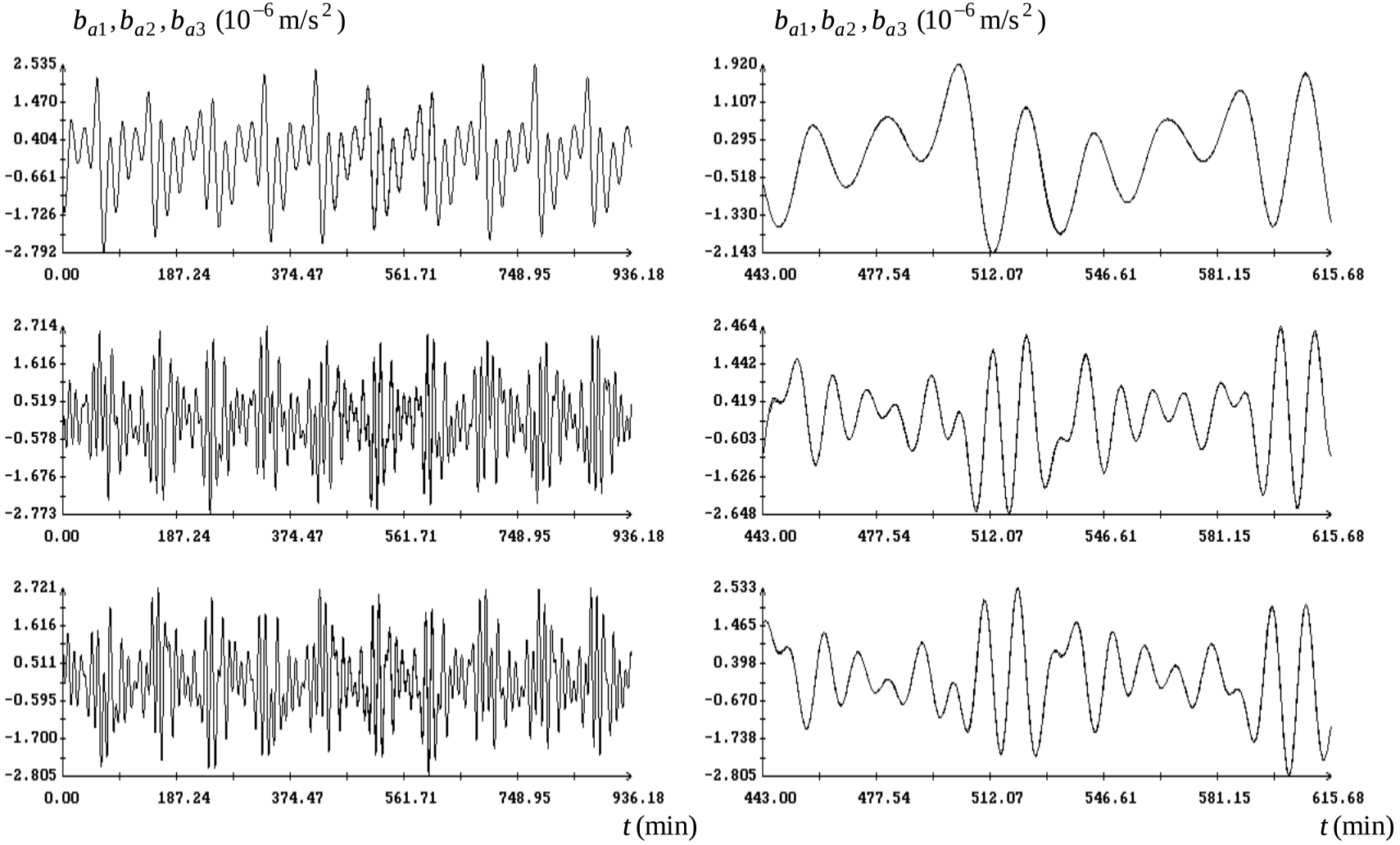

Fig. 4e. Mating of the data from the files ac24_09_37.pas and ac24_17_02.pas. The components of the aerodynamic part of the acceleration. The instant $t = 0$ in the plots corresponds to 09:37:14 UTC 24.09.2007.

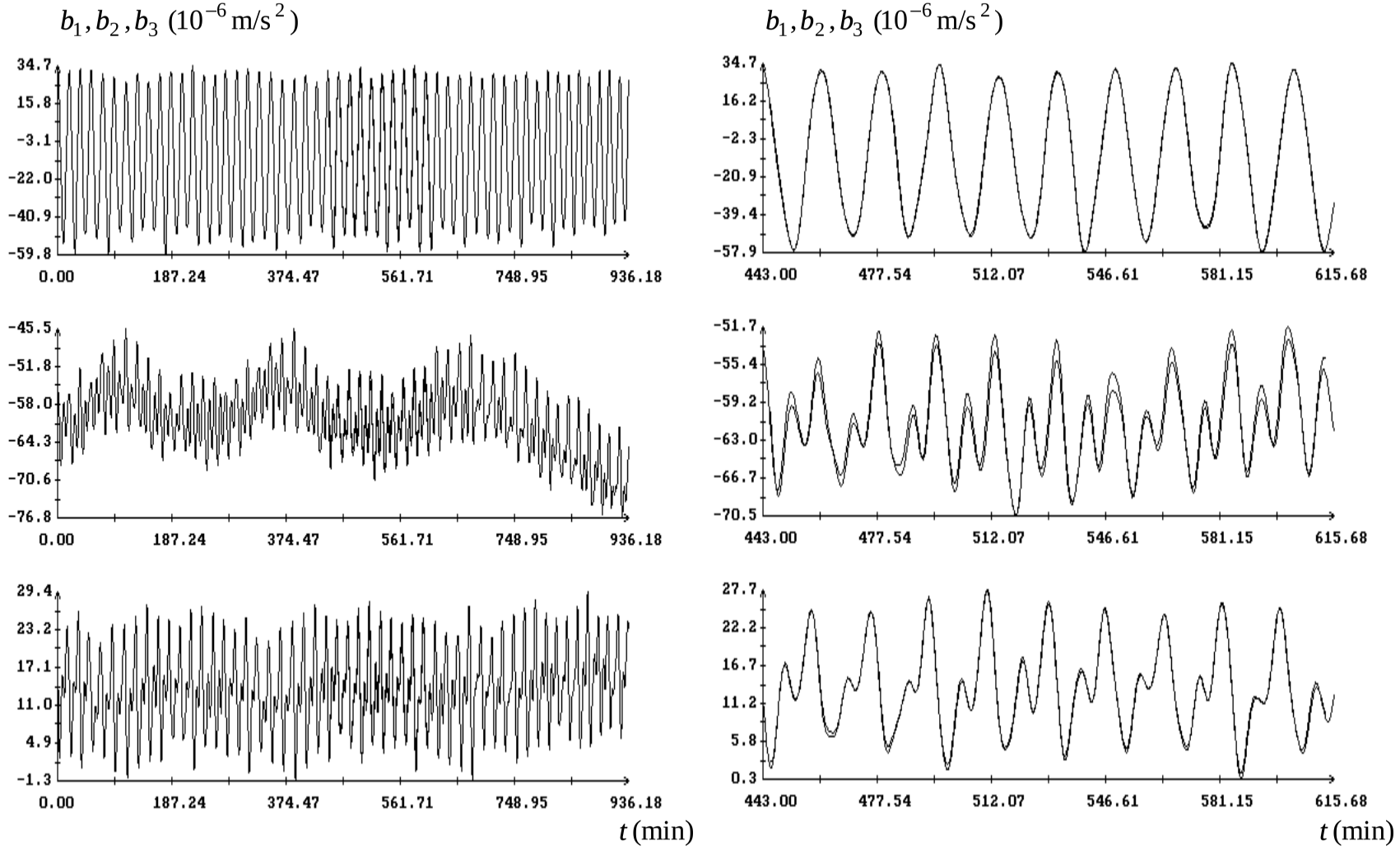

Fig. 4f. Mating of the data from the files ac24_09_37.pas and ac24_17_02.pas. The components of the acceleration at the point $P = (-1\text{m}, -0.9\text{m}, 0.2\text{m})$. The instant $t = 0$ in the plots corresponds to 09:37:14 UTC 24.09.2007.